

**ANALYSIS AND PREDICTION OF STORM WATER LEVELS IN
DELAWARE INLAND BAYS**

BY

MICHELE STRAZZELLA, NOBUHISA KOBAYASHI, AND TINGTING ZHU

RESEARCH REPORT NO. CACR-19-03

April 2019



CENTER FOR APPLIED COASTAL RESEARCH

Ocean Engineering Laboratory
University of Delaware
Newark, Delaware 19716

TABLE OF CONTENTS

LIST OF TABLES.....	ii
FLIST OF FIGURES.....	ii
ABSTRACT.....	v
Chapter	
1 INTRODUCTION.....	1
2 AVAILABLE DATA.....	2
2.1 Tide Gauge Data.....	2
2.2 River Discharge Data.....	31
2.3 Offshore Wave Data.....	33
3 ANALYTICAL MODEL.....	36
3.1 Governing Equations.....	36
4 MODEL CALIBRATION.....	38
5 MODEL ACCURACY.....	42
6 WAVE OVERTOPPING.....	45
7 CONCLUSIONS.....	47
REFERENCES.....	48

LIST OF TABLES

Table 2.1	Peak water level (NAVD88) at Gauge L, I, R, D, B, O, F, and S for 34 storms with date and analytical surge duration T_s	5
Table 2.2	Daily mean discharge at Millsboro Pond Outlet.....	32
Table 2.3	Spectral significant wave height H_{m0} , spectral peak period T_p , and wave angle θ (positive clockwise) from the normal to the straight barrier beach shoreline at the time of the peak water elevation η_m at Lewes.....	35
Table 6.1	Estimated Peak Wave Overtopping Rate Q_m at Gauge I, R, D, O, F, and S during Strom 20.....	46

LIST OF FIGURES

Figure 2.1	Tide gauge data (stars) at locations of Gauge L, D, I, R, B, S, F, and O.....	2
Figure 2.2	Tide gauge data at locations of Gauge L, D, I, R, B, S, F, and O. Wave data at WIS stations, and barrier beach profiles along 14 cross-shore lines (L1 to L14). Map created using Google Earth® software by Google.....	3
Figure 2.3	3-day time series of water level Gauge L, O, S and F for Storm 1, 2, and 3 where daily maximum elevations at Gauge S and F are plotted in the middle of each day.....	7
Figure 2.4	3-day time series of water level Gauges L, O, S and F for Storms 4, 5 and 6 where daily maximum elevations at Gauge S and F are plotted in the middle of each day.....	8
Figure 2.5	3-day time series of water levels at Gauges L, O, S and F for Storms 7, 8 and 9 where daily maximum elevations at Gauge S and F are plotted in the middle of each day.....	9
Figure 2.6	3-day time series of water levels at Gauges L, O, S and F for Storms 10, 11 and 12...	10
Figure 2.7	3-day time series of water levels at Gauges L, O, S and F for Storms 13, 14 and 15....	11
Figure 2.8	3-day time series of water level at Gauges L, O, S and F for Storms 16, 17 and 18....	12
Figure 2.9	3-day time series of water levels at Gauges L, O, S and F for Storms 19, 20 and 21...	13

Figure 2.10	3-day time series of water levels at Gauges L, O, S and F for Storms 22, 23 and 24...	14
Figure 2.11	3-day time series of water levels at Gauges L, O, S and F for Storms 25, 26 and 27...	15
Figure 2.12	3-day time series of water levels at Gauges L, O, S and F for Storms 28, 29 and 30...	16
Figure 2.13	3-day time series of water levels at Gauges L, O, S and F for Storms 31, 32 and 33...	17
Figure 2.14	3-day time series of water levels at Gauges L, O, S and F for storms 34.....	18
Figure 2.15	3-day time series of water levels at Gauges L, I, R and D for Storms 1, 2 and 3 where daily maximum and minimum levels at gauges I, R and D are plotted in the middle of each day.....	19
Figure 2.16	3-day time series of water levels at Gauges L, I, R and D for Storms 4, 5 and 6 where daily maximum and minimum levels at gauges I, R and D are plotted in the middle of each day.....	20
Figure 2.17	3-day time series of water levels at Gauges L, I, R and D for Storms 7, 8 and 9 where daily maximum and minimum levels at gauges I, R and D are plotted in the middle of each day.	21
Figure 2.18	3-day time series of water level at Gauges L, I, R and D for Storms 10, 11 and 12.....	22
Figure 2.19	3-day time series of water level at Gauges L, I, R and D for Storms 13, 14 and 15.....	23
Figure 2.20	3-day time series of water level at Gauges L, I, R and D for Storms 16, 17 and 18 where no data at Gauge I for Storms 16, 17, and 18, and at Gauge R for Storm 17...	24
Figure 2.21	3-day time series of water levels at Gauges L, I, R, and D for Storms 19, 20 and 21.....	25
Figure 2.22	3-day time series of water levels at Gauges L, I, R, and D for Storms 22, 23 and 24...	26
Figure 2.23	3-day time series of water levels at Gauges L, I, R, and D for Storms 25 and 26.....	27
Figure 2.24	3-day time series of water levels at Gauges L, I, R, D and B for Storms 27, 28, and 29.	28
Figure 2.25	3-day time series of water levels at Gauges L, I, R, D and B for Storms 30, 31, and 32.	29
Figure 2.26	3-day time series of water levels at Gauges L, I, R, D and B for Storms 33 and 34.....	30

Figure 2.27	Location of Millsboro Pond Outlet.....	31
Figure 2.28	3-day time series of water elevation η_o at tide gauge L, and the wave height H_{mo} period T_p , and angle θ at WIS 63160 station for storm 20.....	33
Figure 4.1	Measured and analytical peak water level ratio (η_p/η_m) as a function of surge steepness parameter η_m^* for range of inlet and bay parameter K^* at Gauge I, R, D, and B.....	39
Figure 4.2	Measured and analytical peak water level ratio (η_p/η_m) as a function of surge steepness parameter η_m^* for range of inlet and bay parameter K^* at Gauge O, F, and S.....	41
Figure 5.1	Measured and analytical peak water level η_p at Gauge I, R, D, and B and RMS relative error E	43
Figure 5.2	Measured and analytical peak water level η_p at Gauge O, F, and S and RMS relative error E	44

ABSTRACT

A simple approach based on an analytical model and available tide gauge data is proposed for the analysis of storm tide damping inside inland bays with complex bathymetry and for the prediction of peak water levels at gauge locations during storms. The approach was applied to eight tide gauges in the vicinity of Inland Bays in Delaware. Peak water levels at the gauge locations were analyzed for 34 storms during 2005-2017. A damping parameter in the analytical model was calibrated for each bay gauge. The calibrated model predicted the peak water levels within errors of about 0.2 m except for Hurricane Sandy in 2012. The analytical model including wave overtopping was used to estimate the peak wave overtopping rate over the barrier beach from the measured peak water level in the adjacent bay.

Chapter 1

INTRODUCTION

Bay flooding is nowadays predicted using numerical storm tide (sum of storm surge and tide) models on fixed bathymetry. Cialone *et al.* (2017) presented the high-performance computational modeling effort of the North Atlantic Coast Comprehensive Study. The model validation was performed by comparing measured and computed water levels at 38 to 60 tide gauge stations for seven storm conditions. The root-mean-square (RMS) errors were 0.14-0.25 m. The model accuracy was dependent on the accuracy of the modeled bathymetry and bottom friction. Low-lying barrier beaches are common along the Atlantic Coast. Inland bays landward of barrier beaches are typically connected with the Atlantic Ocean through tidal inlets. The spatial variation of bathymetry and bottom friction in such bays can be very complex and difficult to quantify accurately. More tide gauges were installed recently in order to assess local flooding risk inside inland bays with complex bathymetry. Kobayashi & Zhu (2017) proposed a simple analytical model to make the best use of available tide gauge data in bays. In this study, the model is applied to Rehoboth Bay, Indian River Bay, and Little Assawoman Bay (Inland Bays) in Delaware. Storm tide in the Atlantic Ocean enters the shallow Inland Bays through two tidal inlets. Eight tide gauge data for 34 storms during 2005-2017 were analyzed using the analytical model to estimate the ocean storm tide propagation and damping through the inlets and ditches. Wave overtopping of the barrier beach occurred during Hurricane Sandy in 2012. The analytical model including wave overtopping was used inversely to estimate the wave overtopping rate from the measured peak water levels at the bay gauges.

Chapter 2

AVAILABLE FIELD DATA

2.1. Tide gauge data

Figures 2.1 and 2.2 shows the locations of eight tide gauges used in this study. Tide gauge data at Lewis (L in Figure 2.1) and Ocean City Inlet (O) were obtained from the U.S Department of Commerce, National Oceanic and Atmospheric Administration (NOAA 2018). These two gauges were included in the validation by Cialone *et al.* (2017). Tide gauge data at Rehoboth Bay at Dewey Beach (D), Indian River Bay Inlet (I), Indian River at Rosedale Beach (R), Bethany Beach (B), South Bethany (S), and Fenwick Island (F) were obtained from the U.S. Geological Survey (USGS 2018).

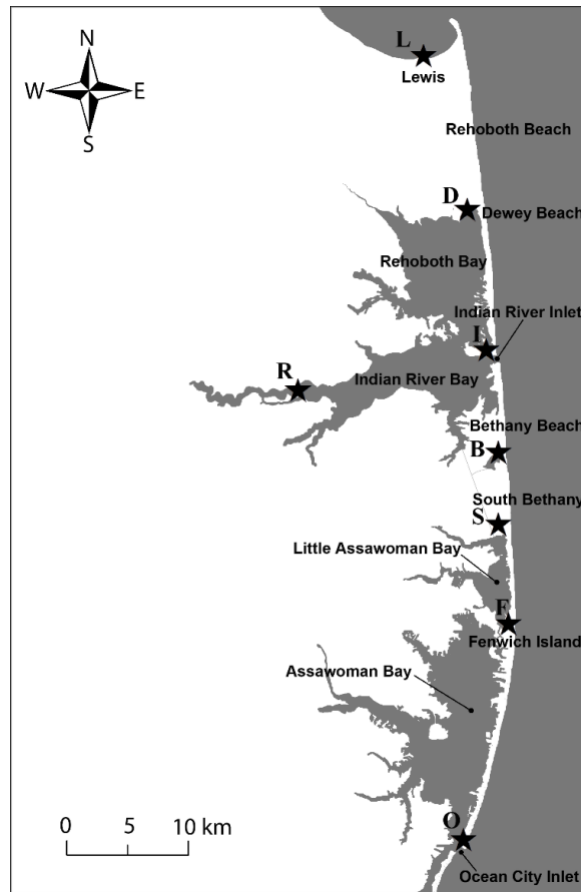


Figure 2.1 Tide gauge data (stars) at locations of Gauge L, D, I, R, B, S, F, and O.



Figure 2.2 Tide gauge data at locations of Gauge L, D, I, R, B, S, F, and O. Wave data at WIS stations, and barrier beach profiles along 14 cross-shore lines (L1 to L14). Map created using Google Earth® software by Google.

Indian River Bay is connected with the Atlantic Ocean through the Indian River Inlet. The inlet depth and width are approximately 20 m and 140 m, respectively. The peak ebb and flood velocities are about 2 m/s and the corresponding peak discharge is about 5,600 m³/s (Kobayashi & Zhu 2017). The tide gauges I and R in Figures 2.1 and 2.2 represent the water level in Indian River Bay. The tide gauge D indicates the water level at the northern end of Rehoboth Bay connected with Indian River Bay through narrow ditches. Indian River Bay and Little Assawoman

Bay are connected through a creek and a canal. The tide gauge B is located in a ditch connected to the canal between the two bays. Little Assawoman Bay is connected with Assawoman Bay through a ditch. The depth and width of the ditch are about 2 m and 140 m, respectively. Storm tide in the Atlantic Ocean propagates through the Ocean City Inlet, Assawoman Bay, and the ditch (Johanson *et al.* 1994). The tide gauge O in Figure 2.1 is located landward of the Ocean City Inlet. The tide gauges F and S represent the water level of Little Assawoman Bay.

The tide gauge L at Lewis situated at the mouth of Delaware Bay may be regarded to represent the water level in the Atlantic Ocean in Figure 2.1. The North American Vertical Datum of 1988 (NAVD88) is used as the datum in this study. The mean higher high water level, mean sea level, and mean lower low water level at Gauge L were 0.62, -0.12, and -0.80 m, respectively. Nadal-Caraballo *et al.* (2016) analyzed the 94-year record of historical extreme water levels of Gauge L. The threshold peak water level for storm events was chosen to be 1.27 m in their statistical analysis. Using the threshold water level of 1.27 m, 34 storms were identified in the record of Gauge L during 2005-2017. This duration was selected on the basis of availability of the other gauge data except that Gauge B was installed in 2015. Each of the 34 storms at Gauge L was characterized by the peak water level η_m exceeding 1.27 m and associated duration T_s . The surge duration T_s was introduced by Kobayashi and Zhu (2017) who analyzed 27 storms during 2005-2015 for Gauge L, I, R, and D. The time series of the water level of Gauge L in the vicinity of the peak (highest) water level was analyzed using zero-crossing points (zero at the datum) and the occurrence time of the low-water level. The surge duration was defined as the duration between the zero-upcrossing point or preceding low-water level time and the zero-downcrossing point or subsequent low-water level time. For the 34 storms, $\eta_m=1.27-2.02$ m and $T_s=7.5-14.5$ h, respectively. Table 2.1 lists the date, the surge duration T_s , and peak water level at Lewis (L) for each of 34 storms and the corresponding peak water level at gauge I, R, D, B, O, F, and S.

Table 2.1 Peak water level (NAVD88) at Gauge L, I, R, D, B, O, F, and S for 34 storms with date and analytical surge duration T_s .

Storm	Peak Date			T_s (h)	Peak Water Level (m)							
	Year	Month	Day		Ocean	Bay						
					L	I	R	D	B	O	F	S
1	2005	5	25	9.4	1.39	1.12	NA	NA	NA	0.83	NA	0.43
2	2005	10	13	13.5	1.32	1.12	1.18	0.81	NA	0.85	0.59	0.55
3	2006	1	31	8.1	1.38	1.03	1.00	NA	NA	0.74	0.35	0.40
4	2006	2	12	12.0	1.32	1.21	1.12	0.73	NA	0.68	0.35	0.39
5	2006	10	7	10.2	1.45	1.27	1.36	0.88	NA	0.86	0.46	0.44
6	2006	11	23	11.1	1.32	1.28	1.26	0.90	NA	1.22	0.51	0.49
7	2007	4	18	8.0	1.28	0.97	0.97	0.46	NA	0.70	0.38	0.43
8	2007	6	13	8.7	1.27	0.98	0.99	0.60	NA	0.67	0.35	0.35
9	2008	5	12	12.6	1.60	1.37	1.41	1.00	NA	0.97	0.62	0.62
10	2008	9	25	12.2	1.29	1.21	1.28	0.74	NA	0.77	0.46	0.50
11	2008	10	19	10.6	1.28	1.20	1.05	0.73	NA	0.72	0.50	0.57
12	2009	10	17	10.8	1.45	1.25	1.29	0.95	NA	0.96	0.64	0.66
13	2009	11	13	11.9	1.60	1.54	1.56	1.10	NA	1.12	0.67	0.68
14	2009	12	19	11.7	1.38	1.19	1.33	0.78	NA	0.76	0.52	0.55
15	2010	3	13	12.3	1.30	1.09	1.19	0.80	NA	0.73	0.65	0.70
16	2011	5	17	7.9	1.27	NA	0.92	0.63	NA	0.68	0.38	0.44
17	2011	8	27	10.7	1.70	NA	NA	0.97	NA	0.93	0.52	0.71
18	2011	10	29	9.9	1.56	NA	1.27	0.79	NA	0.86	0.47	0.47
19	2012	6	5	8.8	1.43	1.03	1.09	0.71	NA	0.80	0.50	0.48
20	2012	10	29	13.4	1.85	1.75	1.66	1.34	NA	1.34	1.23	1.42
21	2013	3	6	14.5	1.45	1.32	1.52	0.81	NA	1.00	0.58	0.58
22	2013	3	9	9.5	1.29	1.08	1.05	0.78	NA	0.77	0.56	0.61
23	2014	1	3	8.1	1.28	0.99	0.96	0.60	NA	0.73	0.36	0.37
24	2014	2	13	10.9	1.30	1.02	1.21	0.59	NA	0.67	0.46	0.52
25	2014	4	30	9.1	1.30	1.01	1.13	0.76	NA	0.68	0.49	0.58
26	2014	12	9	11.6	1.36	1.09	1.22	0.94	NA	0.84	0.55	0.57
27	2015	10	2	12.7	1.51	1.26	1.48	0.95	0.83	0.94	0.60	0.54
28	2016	1	23	13.3	2.02	1.42	1.74	1.09	0.85	0.99	0.62	0.67
29	2016	2	9	9.7	1.41	1.09	1.21	0.92	0.56	0.81	0.59	0.65
30	2016	5	5	8.5	1.30	0.92	1.13	0.74	0.45	0.71	0.49	0.53
31	2016	9	29	12.4	1.35	1.09	1.48	0.97	0.77	0.84	0.69	0.70
32	2017	1	23	12.5	1.36	1.19	1.45	1.00	0.76	0.91	0.73	0.71
33	2017	3	14	7.5	1.33	0.86	0.90	0.50	0.27	0.53	0.25	0.21
34	2017	9	19	10.8	1.41	1.12	1.25	0.89	0.58	0.86	0.62	0.64
			Max	14.5	2.02	1.75	1.74	1.34	0.85	1.34	1.23	1.42
			Min	7.5	1.27	0.86	0.90	0.46	0.27	0.53	0.25	0.21

The water levels of the other gauges in the bays were examined for the duration of three days for each of the 34 storms, starting from one day before the date of the peak water level of Gauge L.

In the Figures 2.3 – 2.14, 3-day time series of the water level at Gauge L, O, F, S starting from one day before the date of each storm listed in Table 2.1. Figures 2.15-2.27 show 3-day time series at Gauge L, I, R, D and B.

- Storms 1, 2, and 3

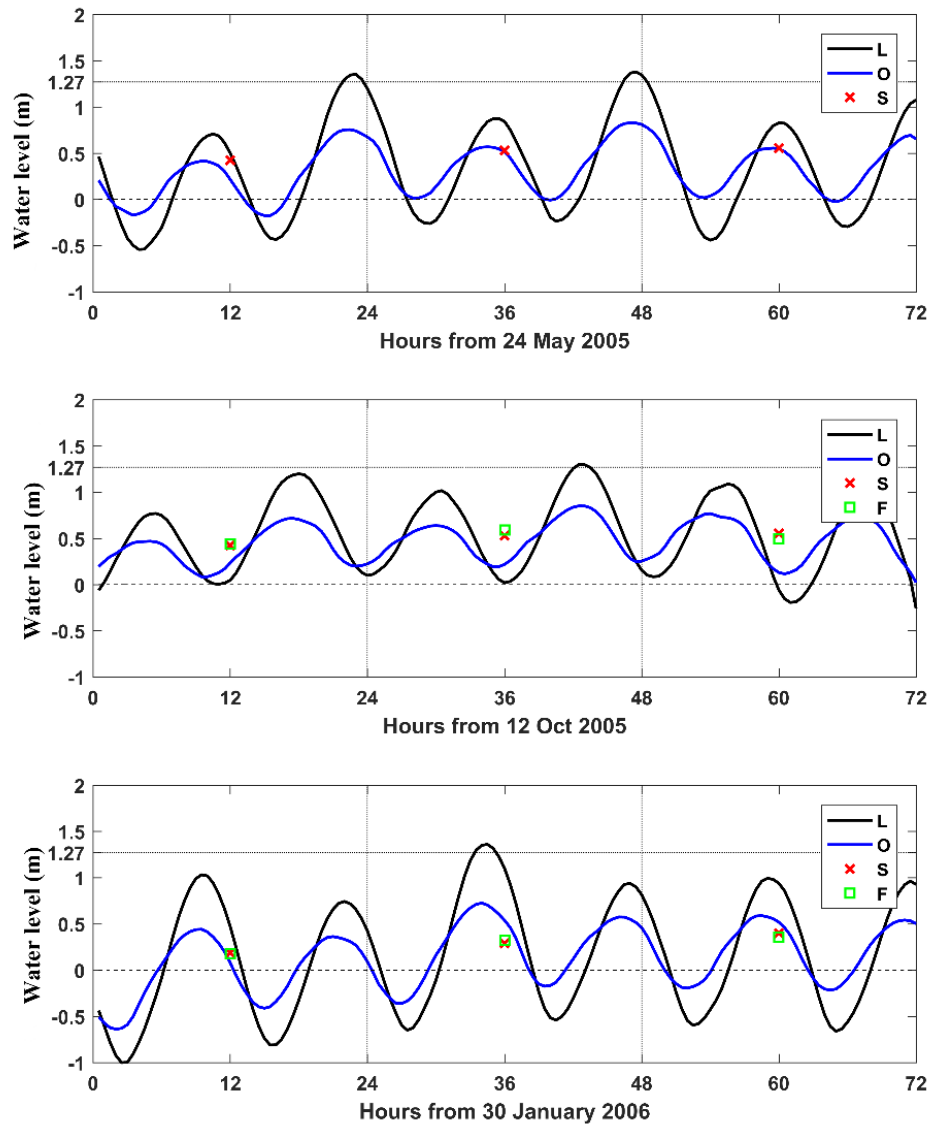


Figure 2.3 3-day time series of water level Gauge L, O, S and F for Storm 1, 2, and 3 where daily maximum elevations at Gauge S and F are plotted in the middle of each day.

- Storms 4, 5, and 6

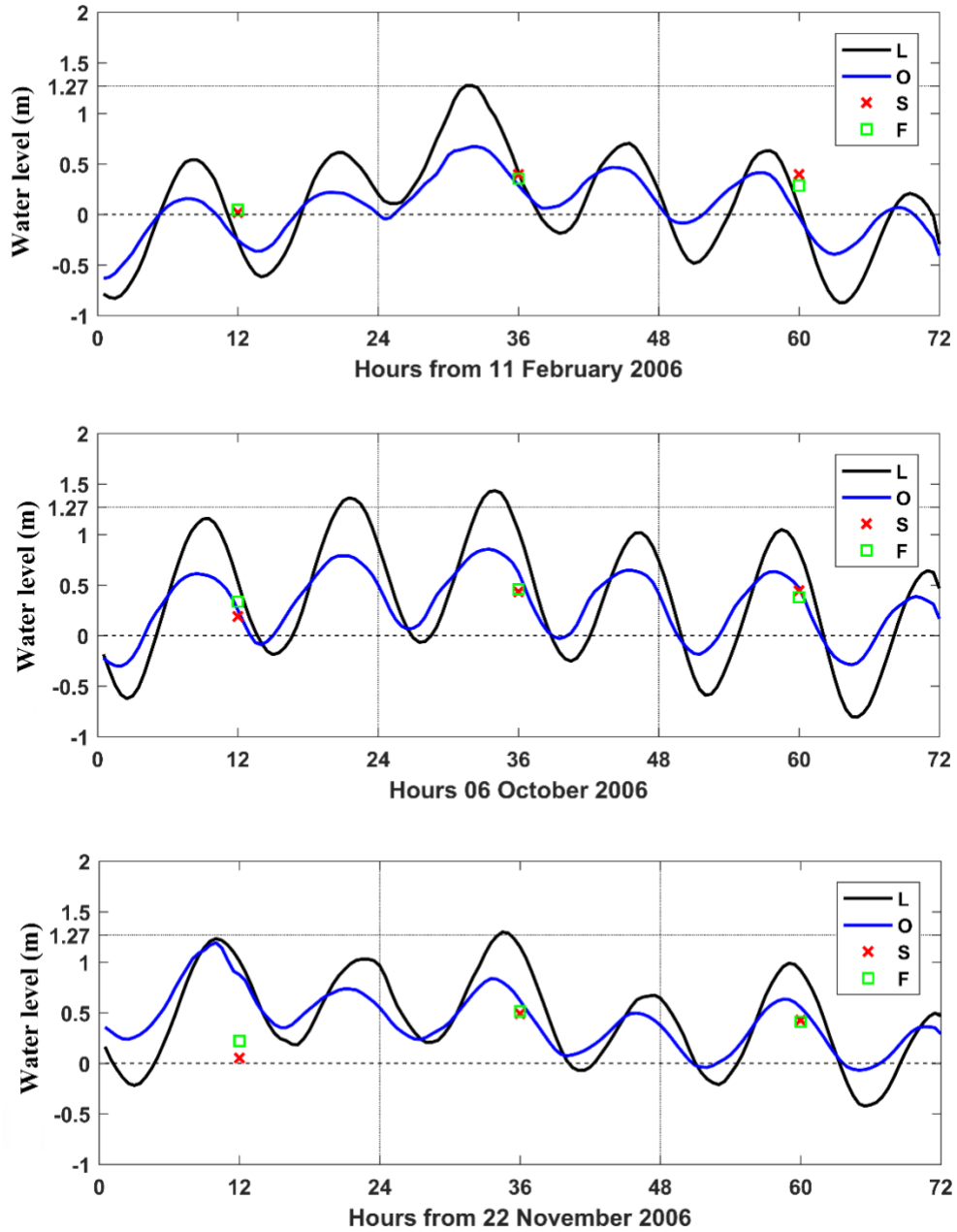


Figure 2.4 3-day time series of water level Gauges L, O, S and F for Storms 4, 5 and 6 where daily maximum elevations at Gauge S and F are plotted in the middle of each day.

- Storms 7, 8, and 9

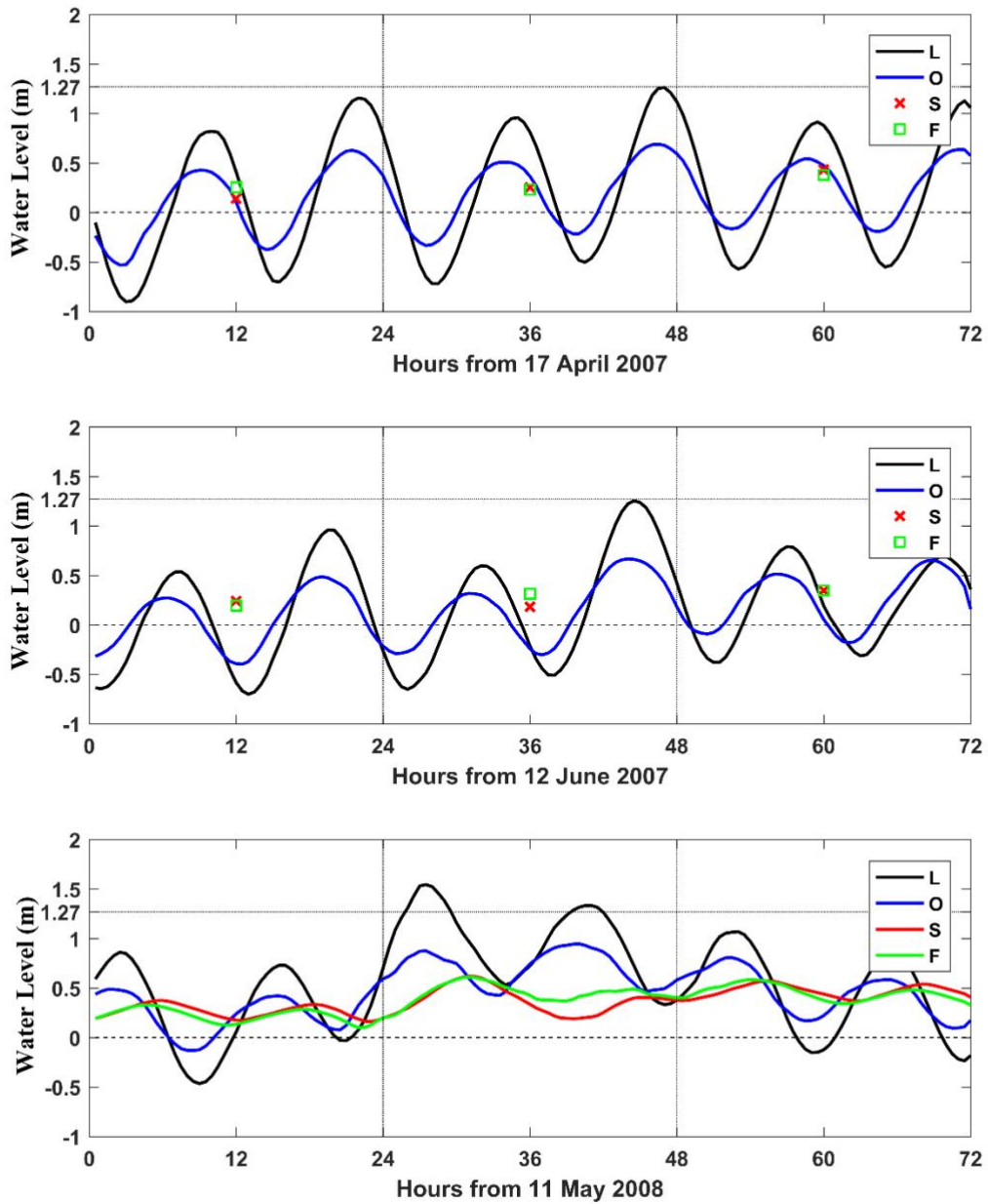


Figure 2.5 3-day time series of water levels at Gauges L, O, S and F for Storms 7, 8 and 9 where daily maximum elevations at Gauge S and F are plotted in the middle of each day.

- Storms 10, 11, and 12

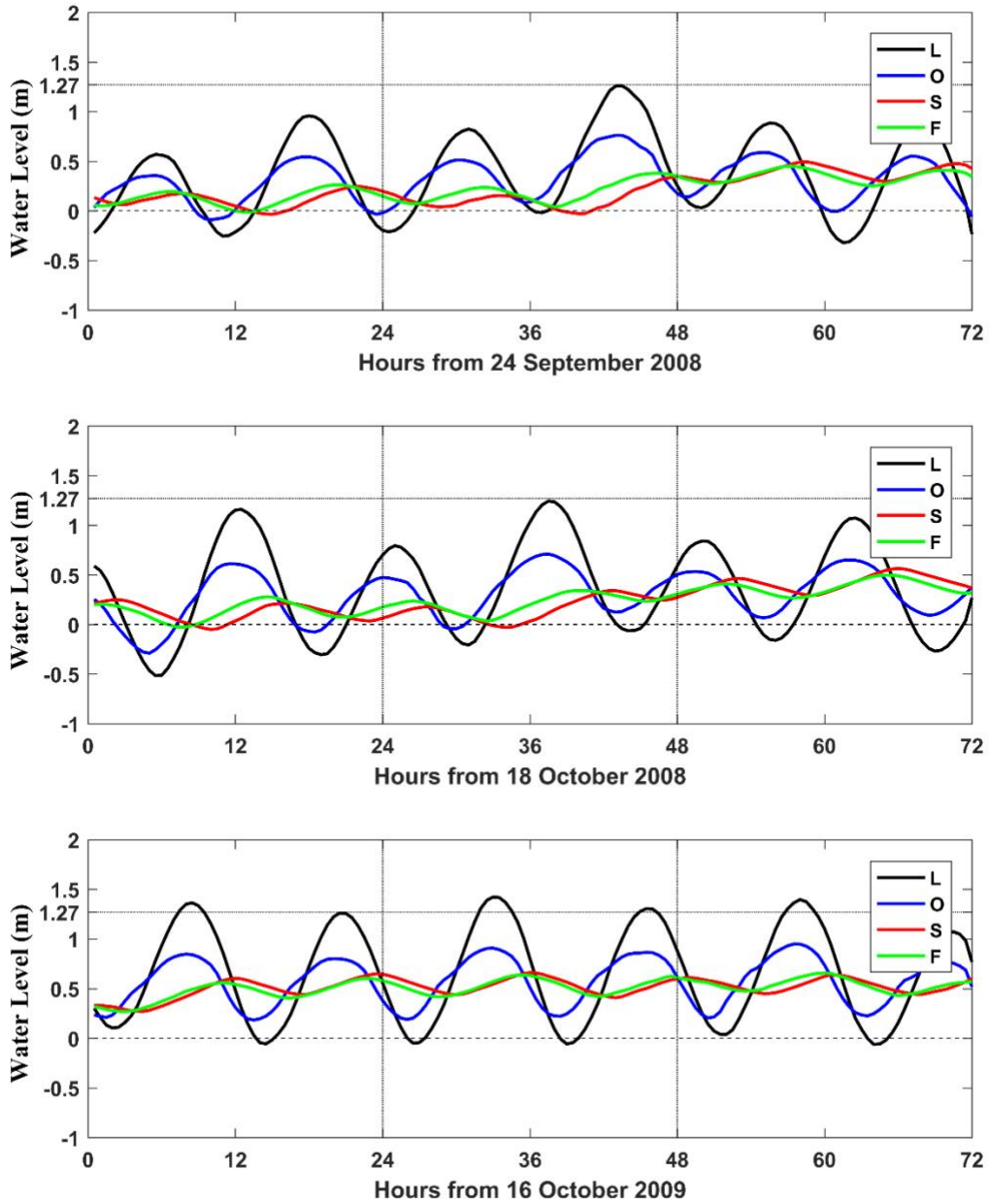


Figure 2.6 3-day time series of water levels at Gauges L, O, S and F for Storms 10, 11 and 12.

- Storms 13, 14, and 15

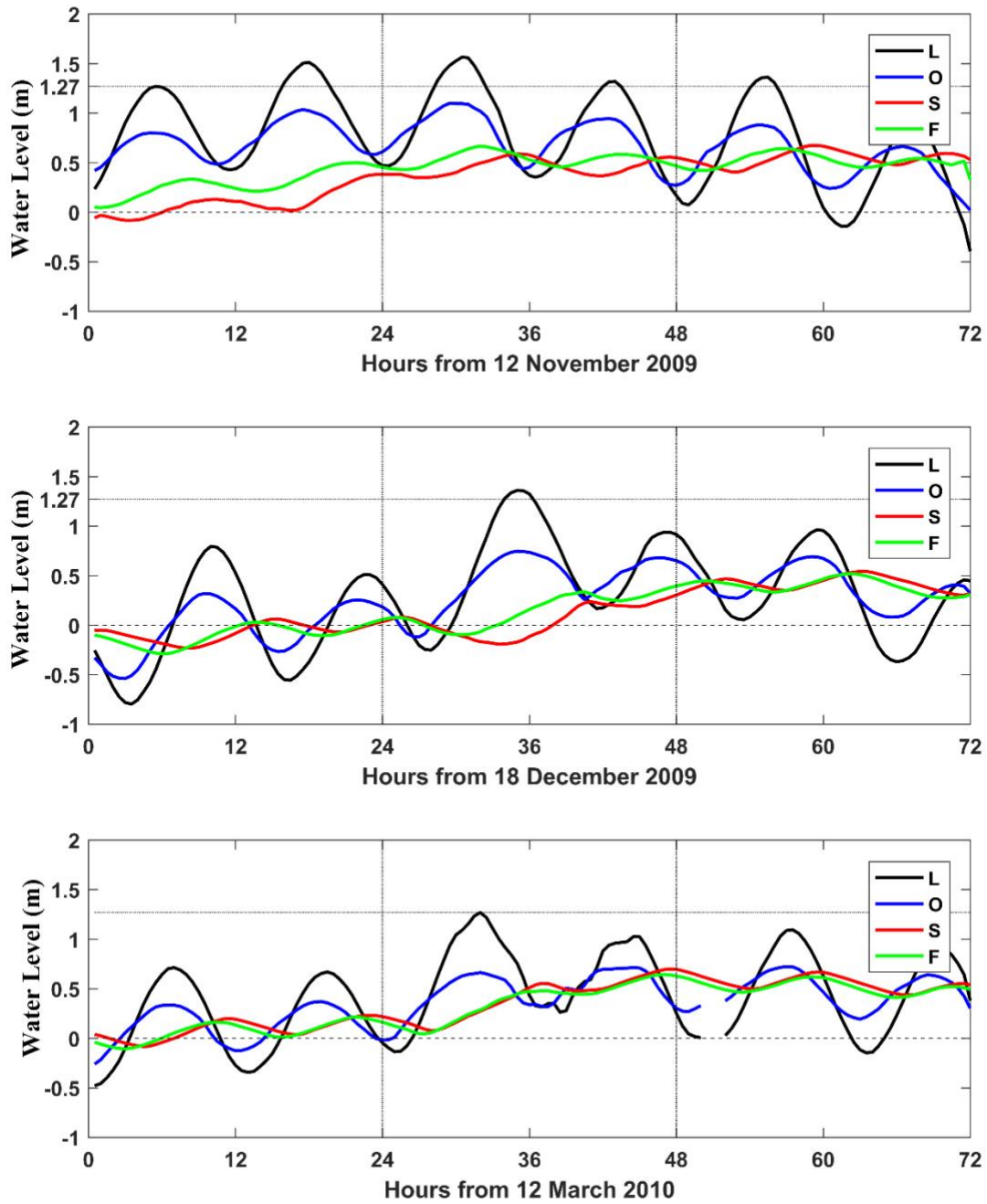


Figure 2.7 3-day time series of water levels at Gauges L, O, S and F for Storms 13, 14 and 15.

- Storms 16, 17, and 18

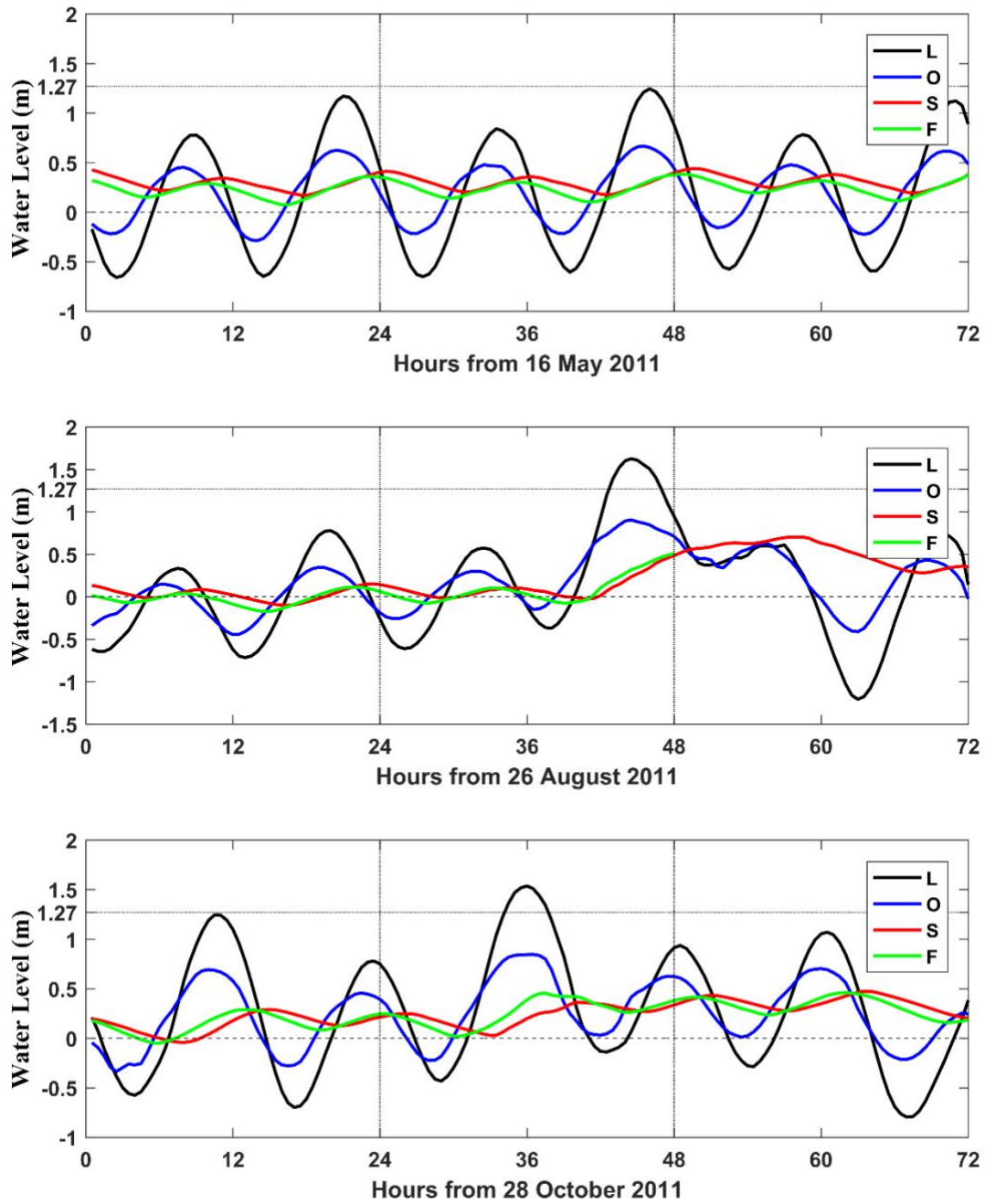


Figure 2.8 3-day time series of water level at Gauges L, O, S and F for Storms 16, 17 and 18.

- Storms 19, 20, and 21

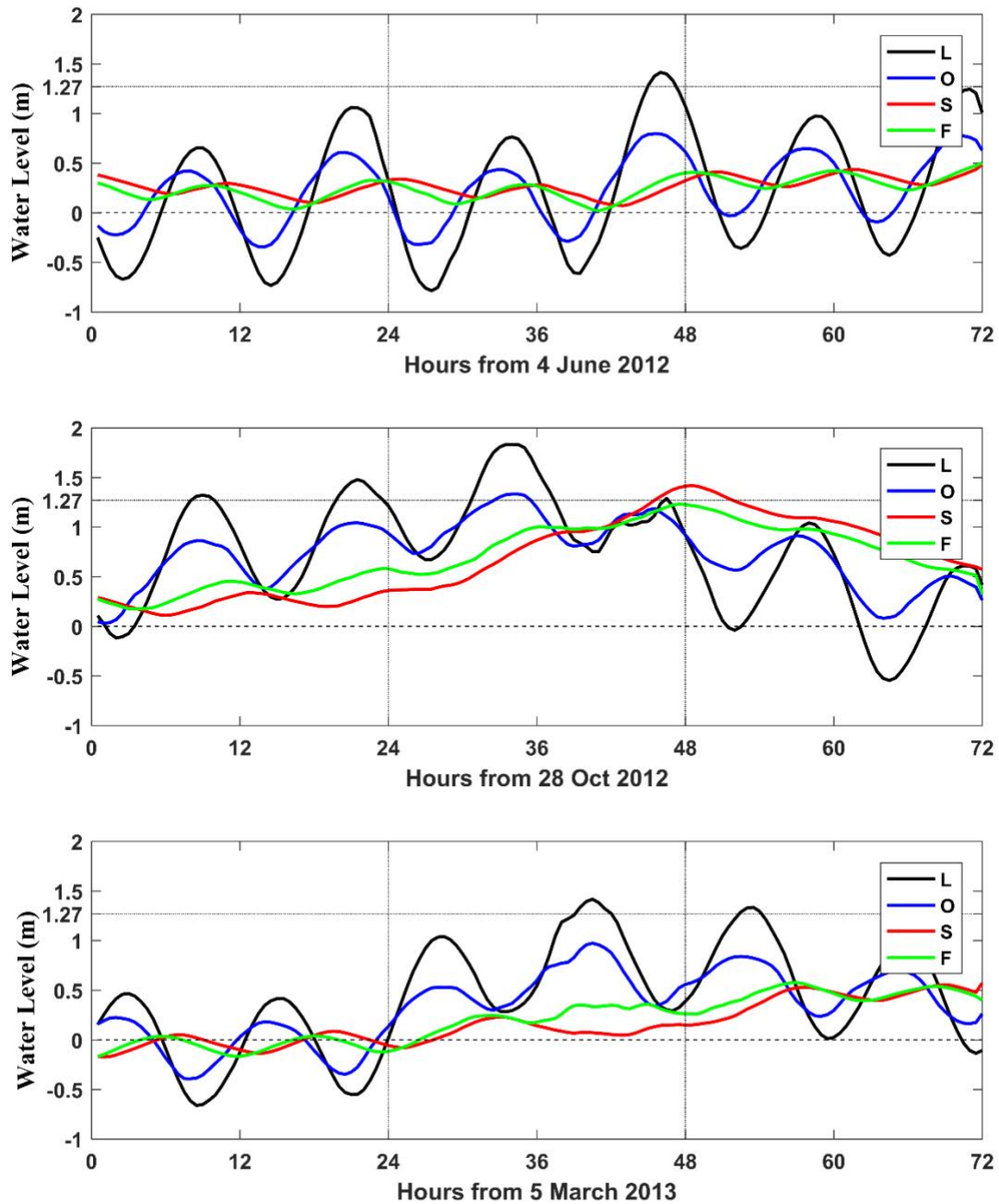


Figure 2.9 3-day time series of water levels at Gauges L, O, S and F for Storms 19, 20 and 21.

- Storms 22, 23, and 24

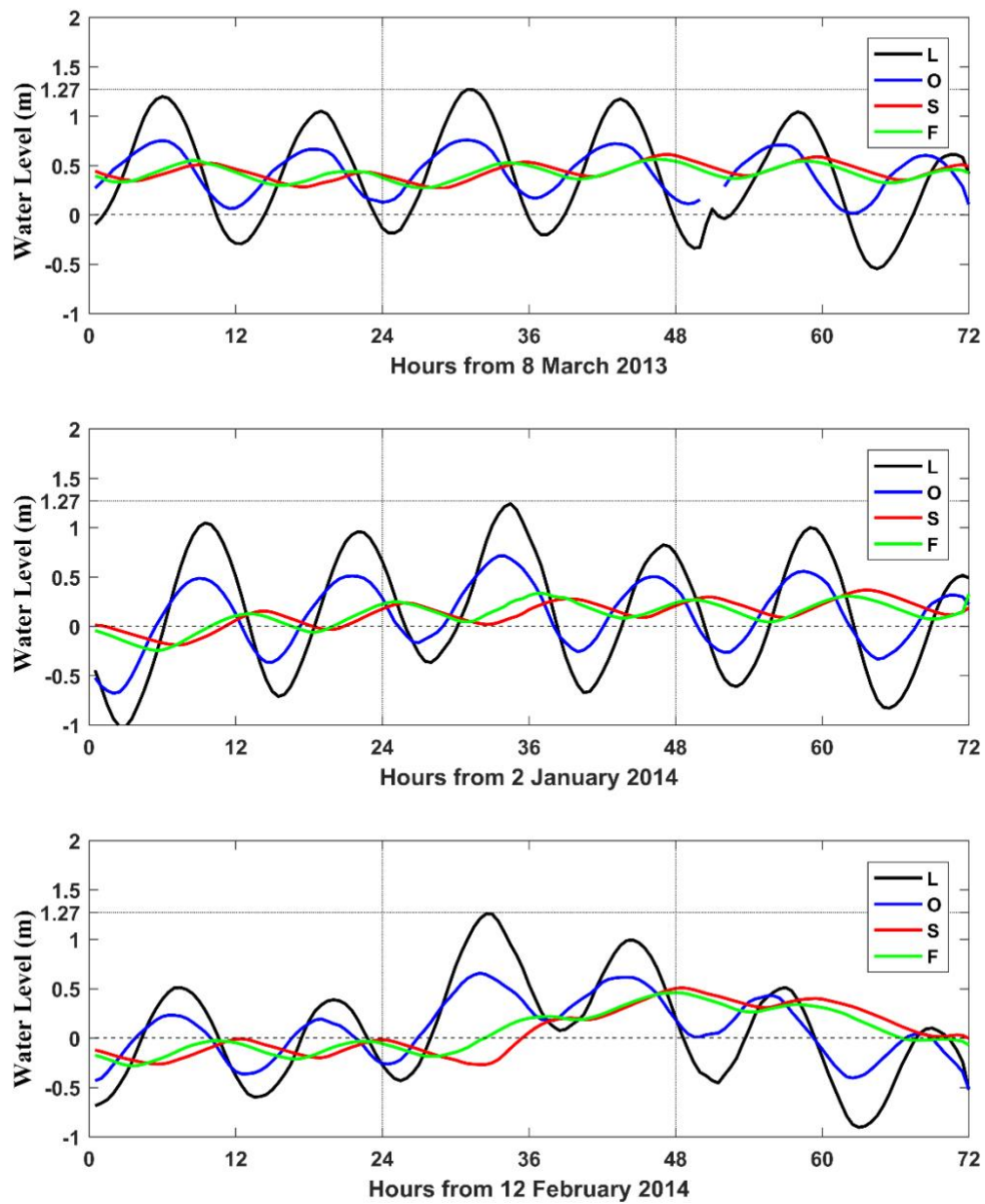


Figure 2.10 3-day time series of water levels at Gauges L, O, S and F for Storms 22, 23 and 24.

- Storms 25, 26, and 27

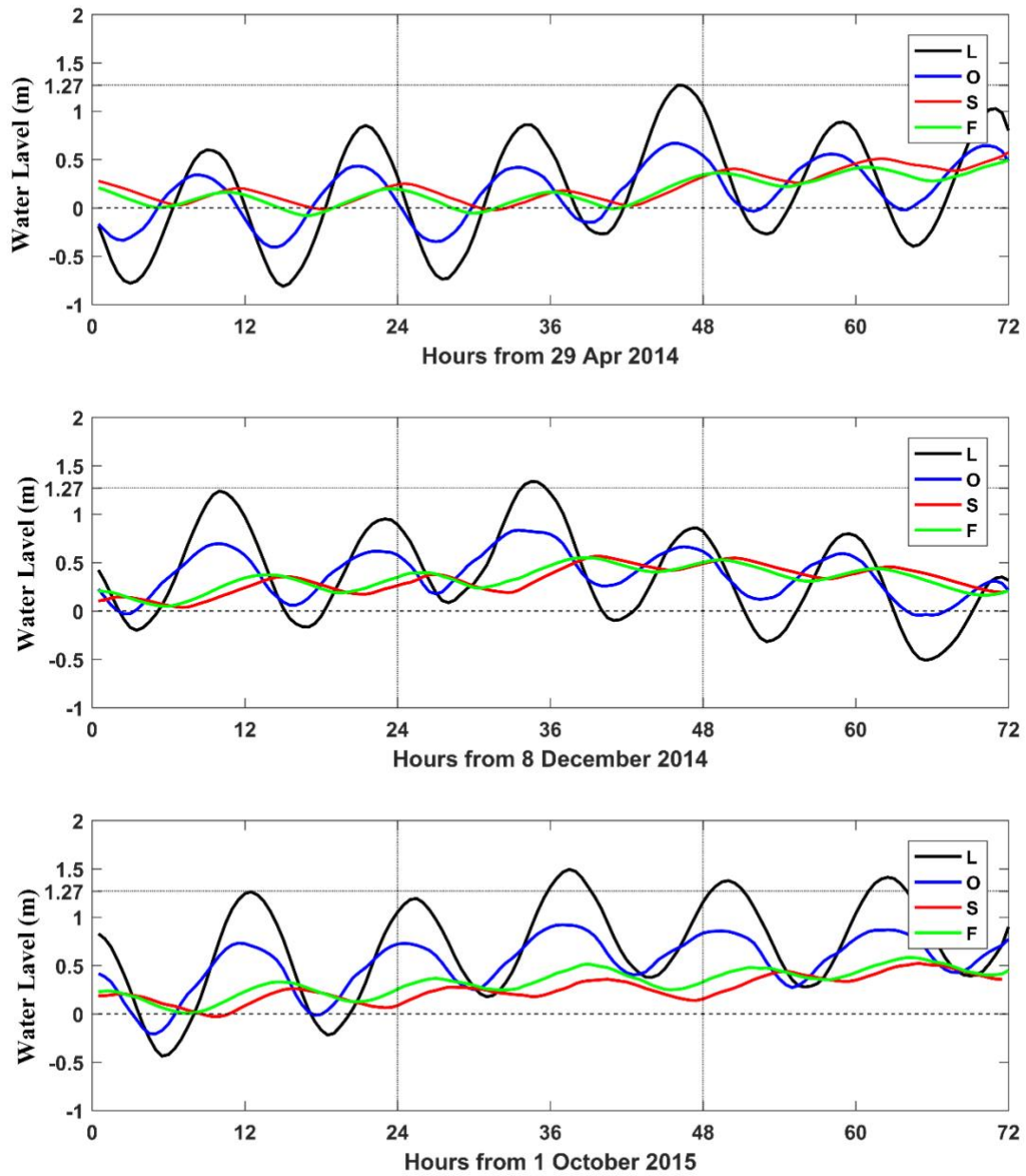


Figure 2.11 3-day time series of water levels at Gauges L, O, S and F for Storms 25, 26 and 27.

- Storms 28, 29, and 30

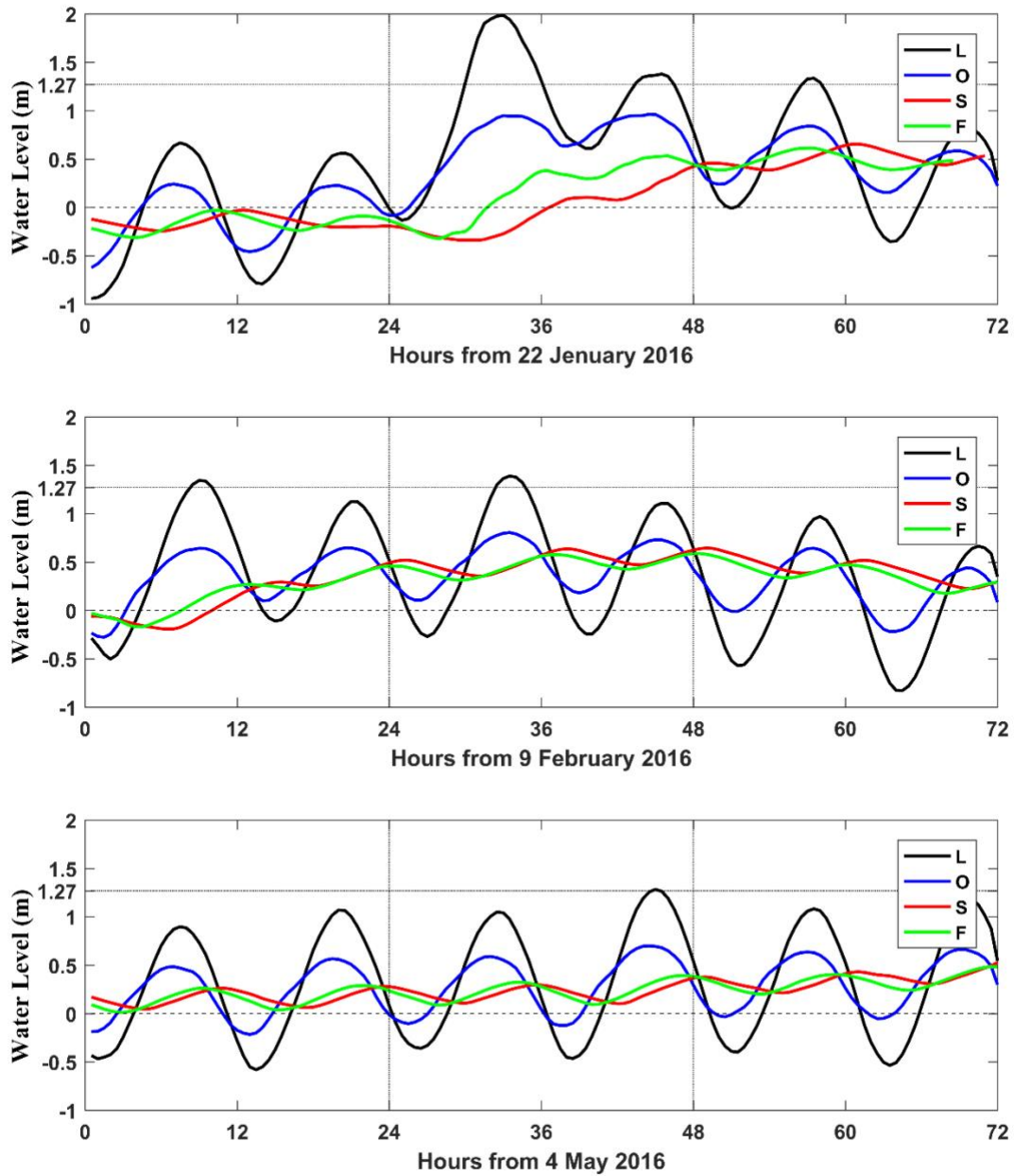


Figure 2.12 3-day time series of water levels at Gauges L, O, S and F for Storms 28, 29 and 30.

- Storms 31, 32, and 33

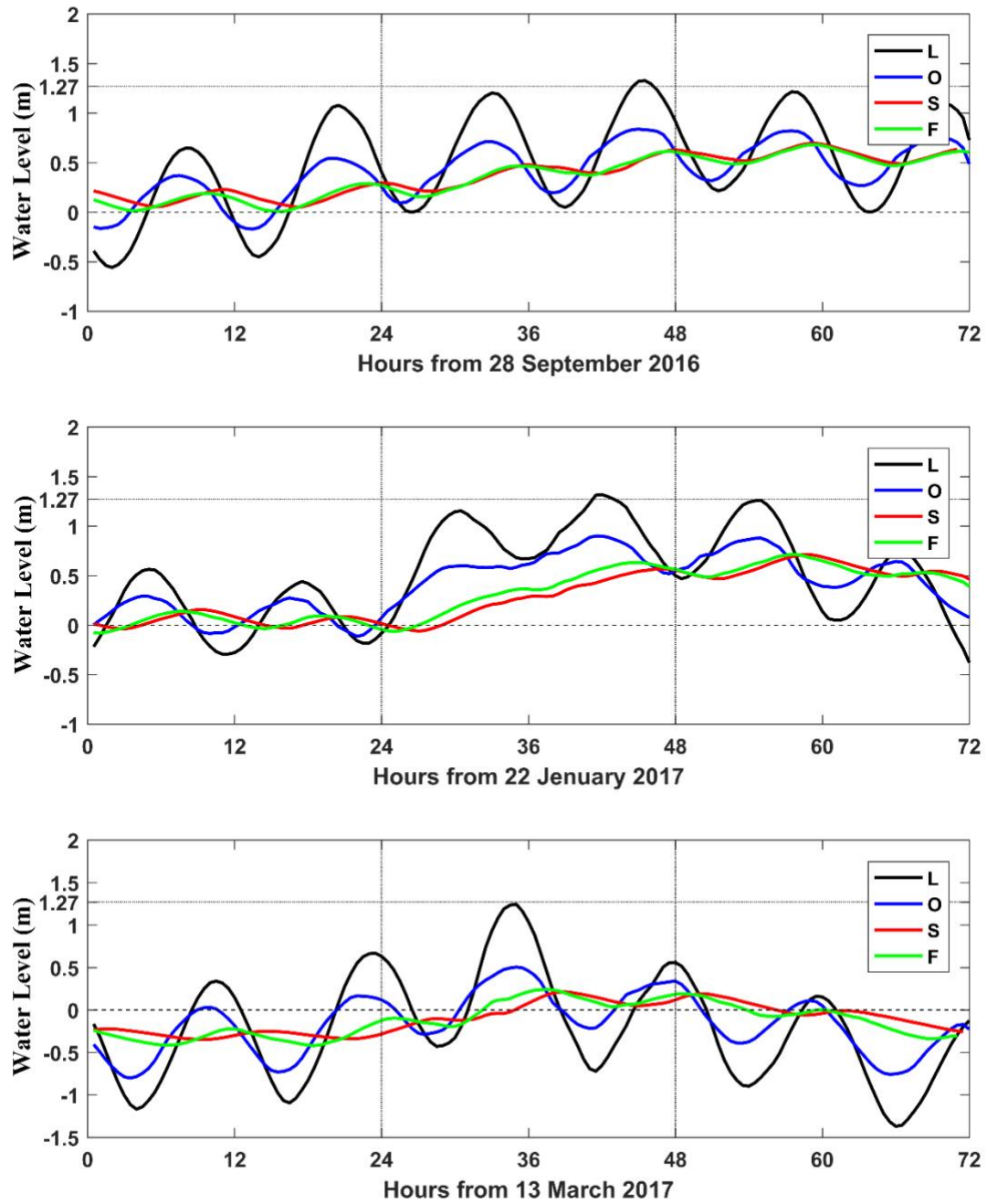


Figure 2.13 3-day time series of water levels at Gauges L, O, S and F for Storms 31, 32 and 33.

- Storm 34

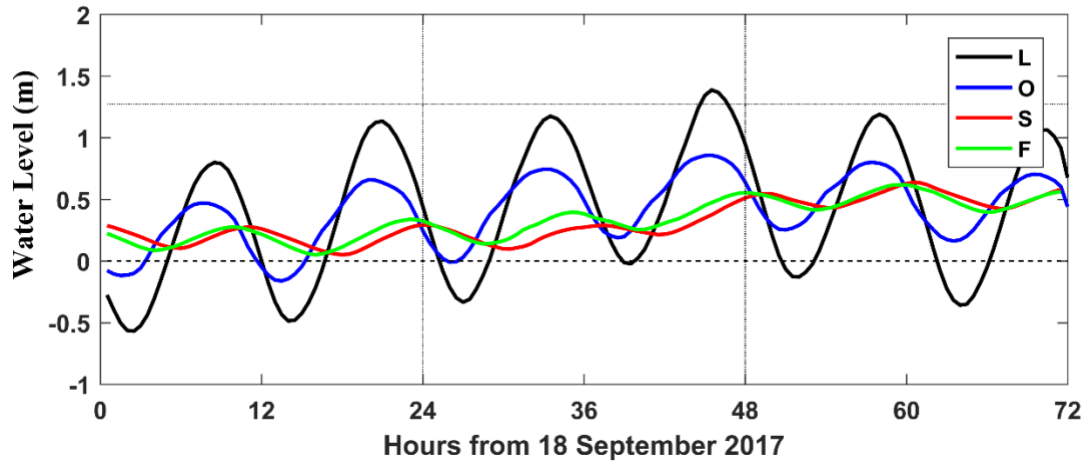


Figure 2.14 3-day time series of water levels at Gauges L, O, S and F for storms 34.

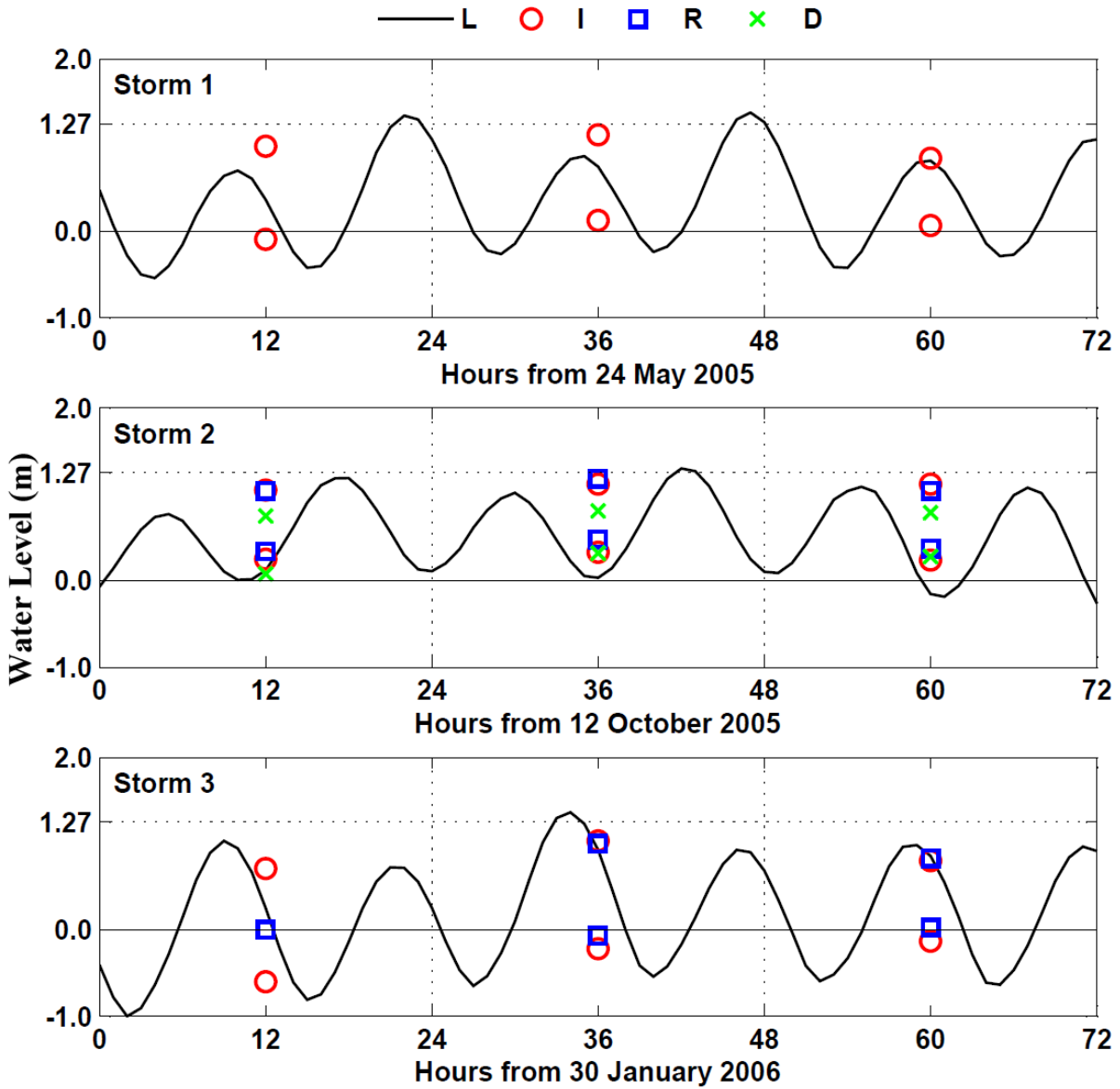


Figure 2.15 3-day time series of water levels at Gauges L, I, R and D for Storms 1, 2 and 3 where daily maximum and minimum levels at gauges I, R and D are plotted in the middle of each day.

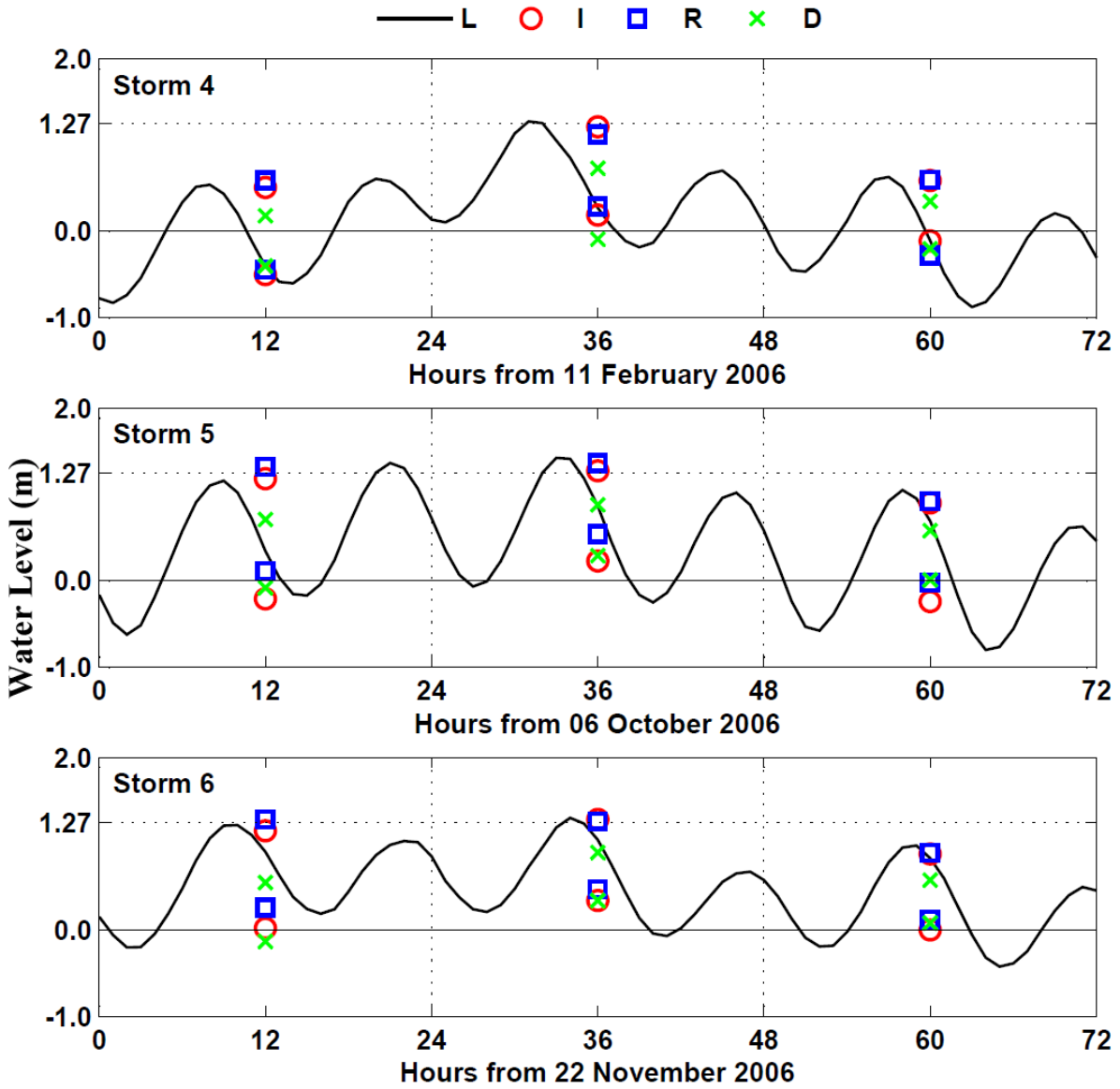


Figure 2.16 3-day time series of water levels at Gauges L, I, R and D for Storms 4, 5 and 6 where daily maximum and minimum levels at gauges I, R and D are plotted in the middle of each day.

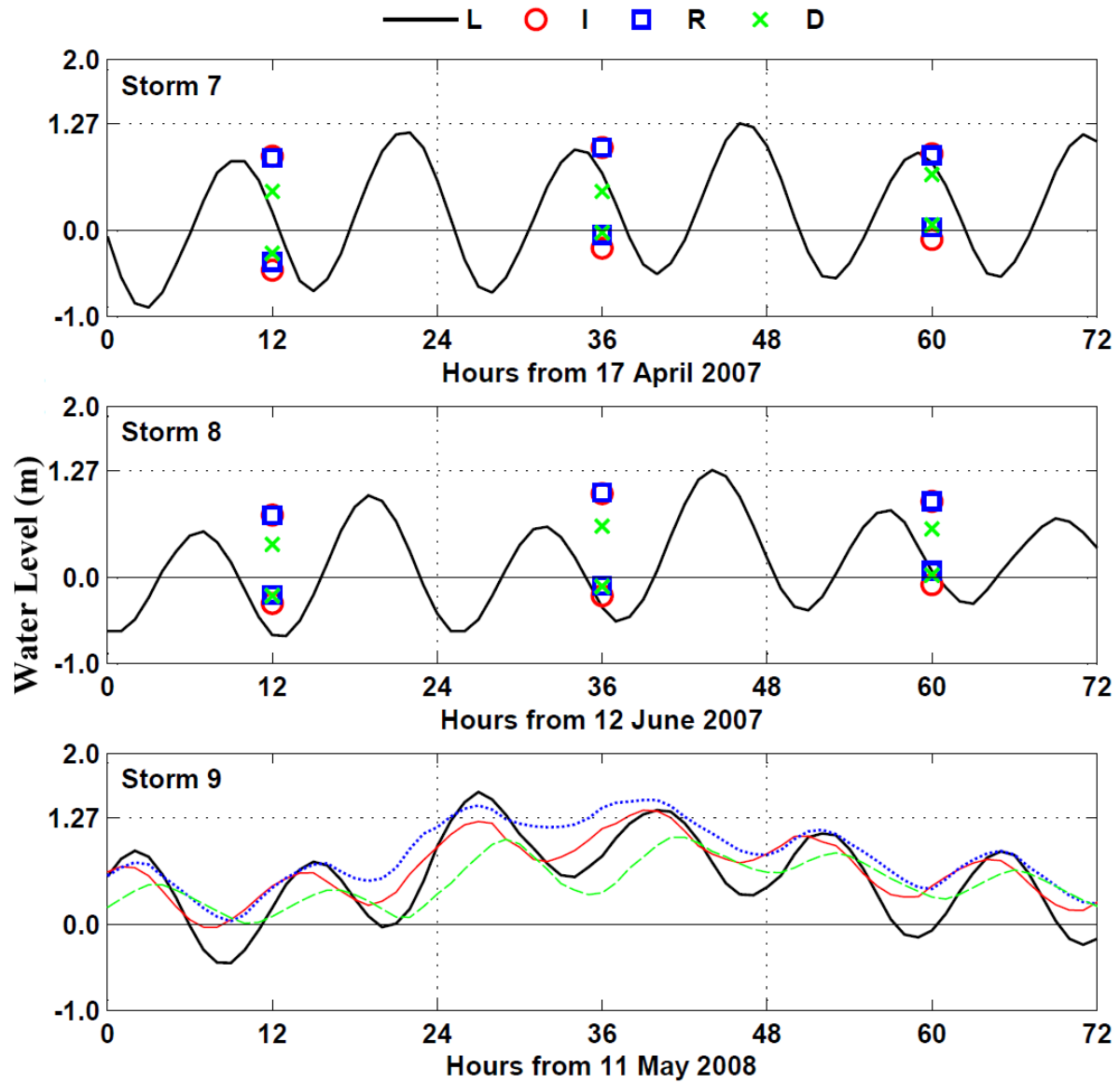


Figure 2.17 3-day time series of water levels at Gauges L, I, R and D for Storms 7, 8 and 9 where daily maximum and minimum levels at gauges I, R and D are plotted in the middle of each day.

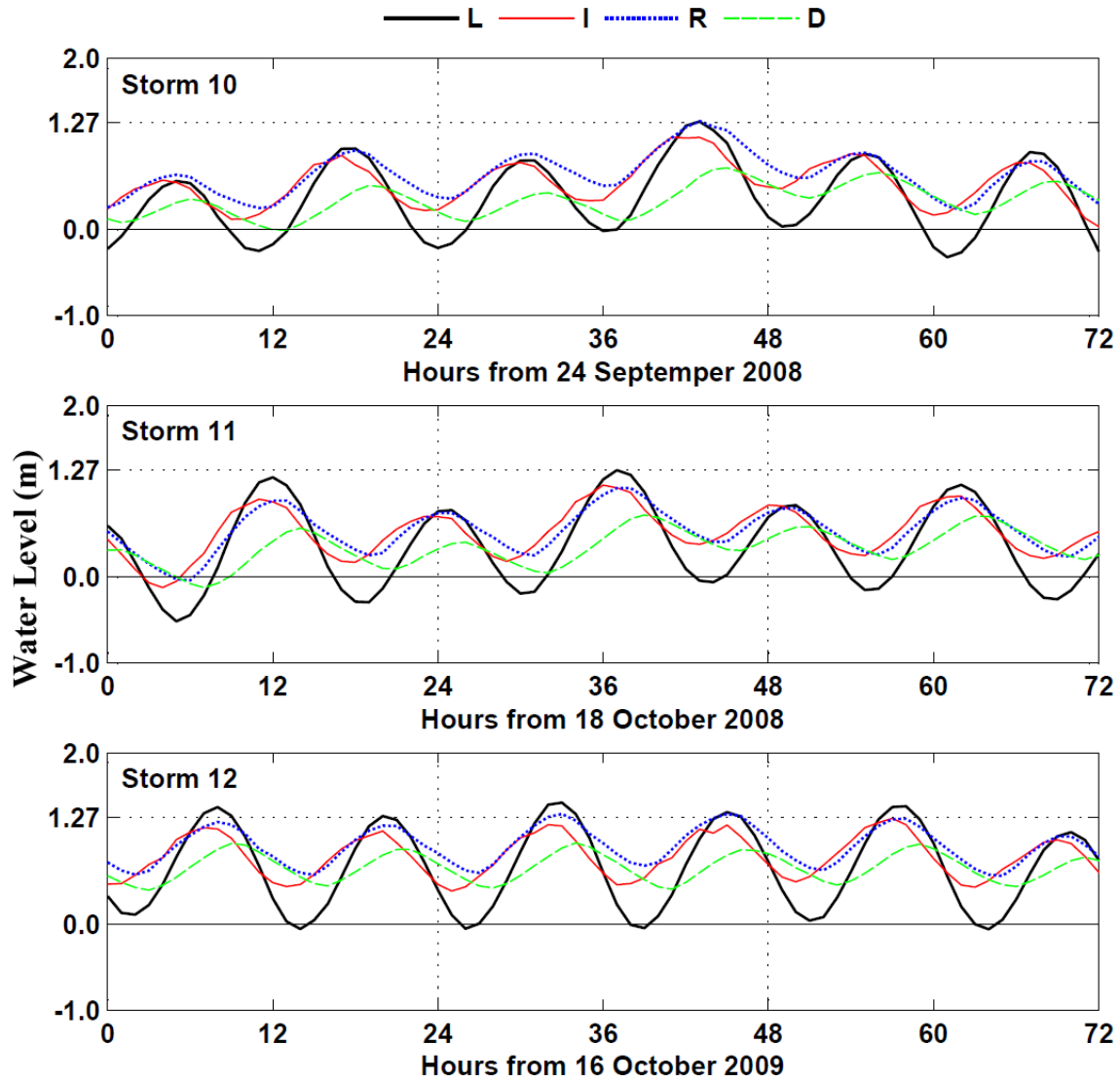


Figure 2.18 3-day time series of water level at Gauges L, I, R and D for Storms 10, 11 and 12.

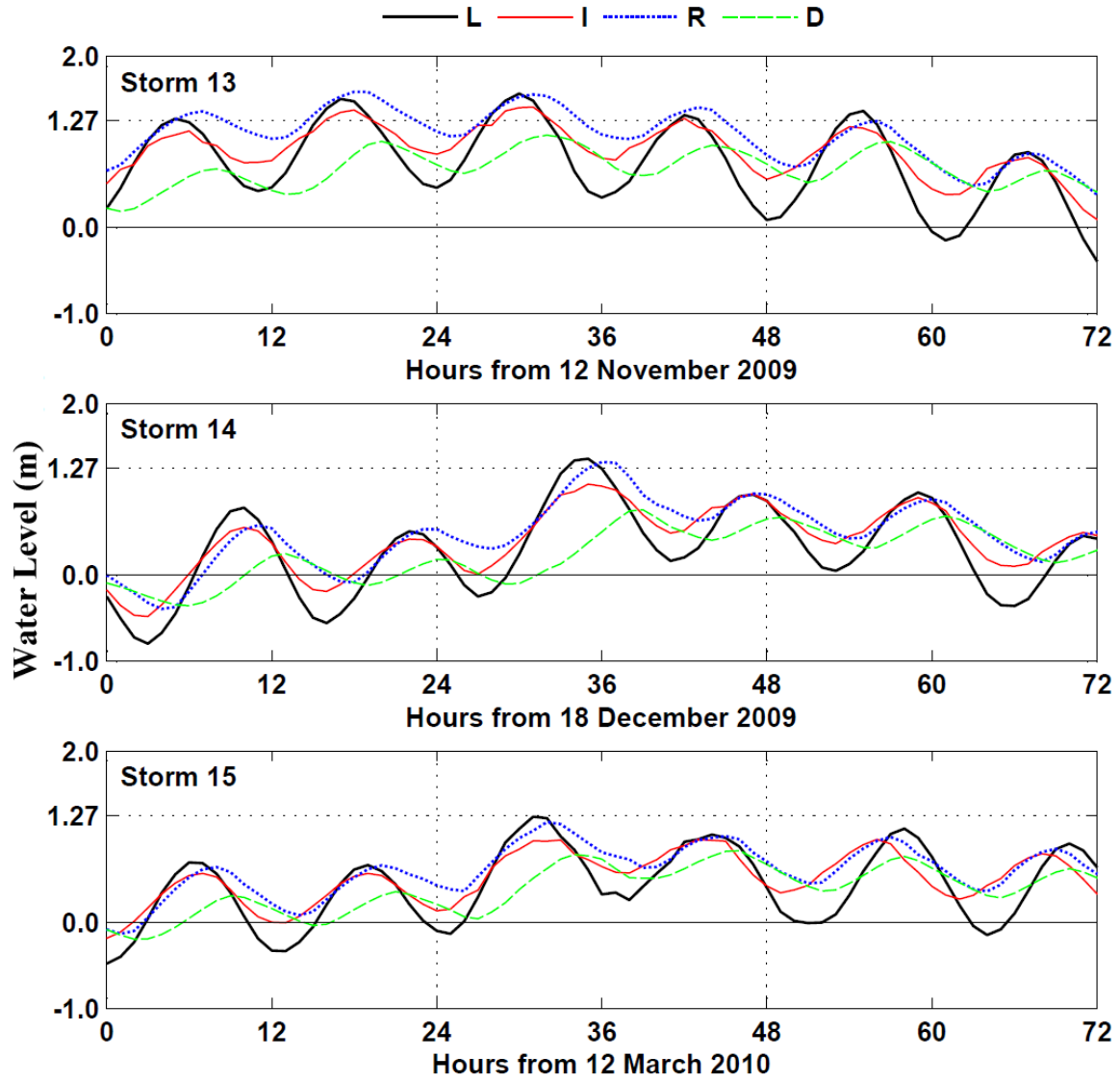


Figure 2.19 3-day time series of water level at Gauges L, I, R and D for Storms 13, 14 and 15.

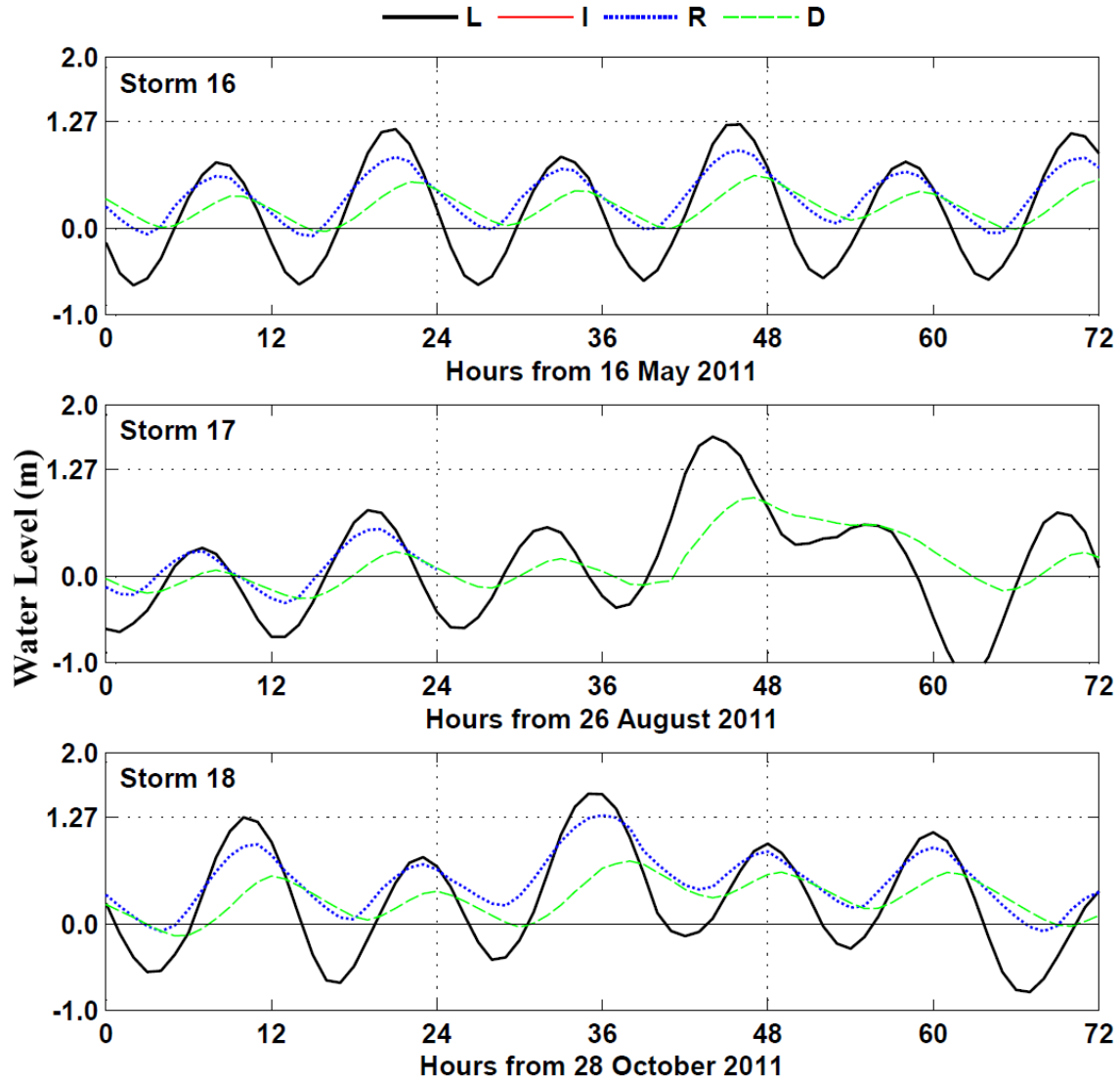


Figure 2.20 3-day time series of water level at Gauges L, I, R and D for Storms 16, 17 and 18 where no data at Gauge I for Storms 16, 17, and 18, and at Gauge R for Storm 17.

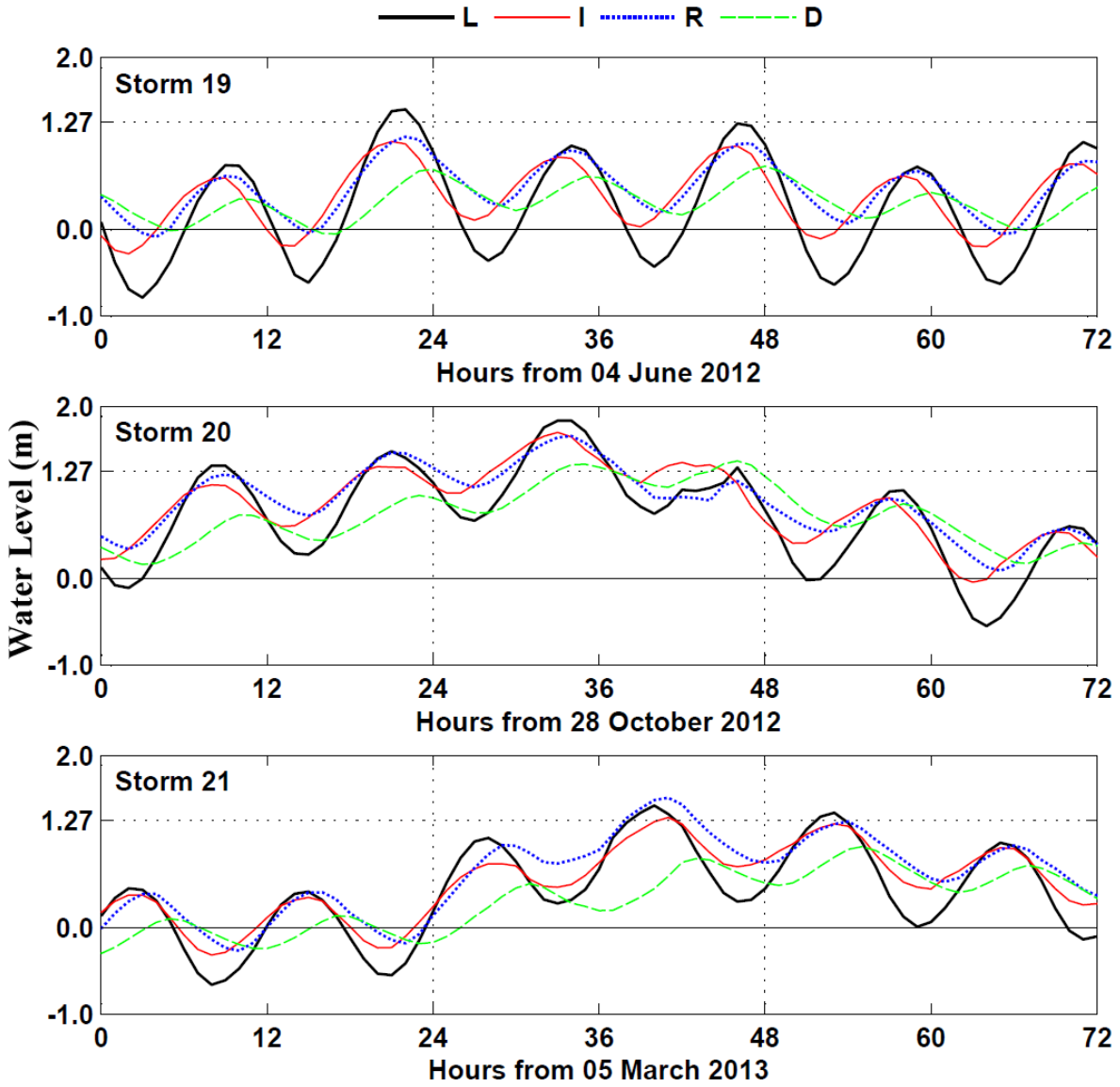


Figure 2.21 3-day time series of water levels at Gauges L, I, R, and D for Storms 19, 20 and 21.

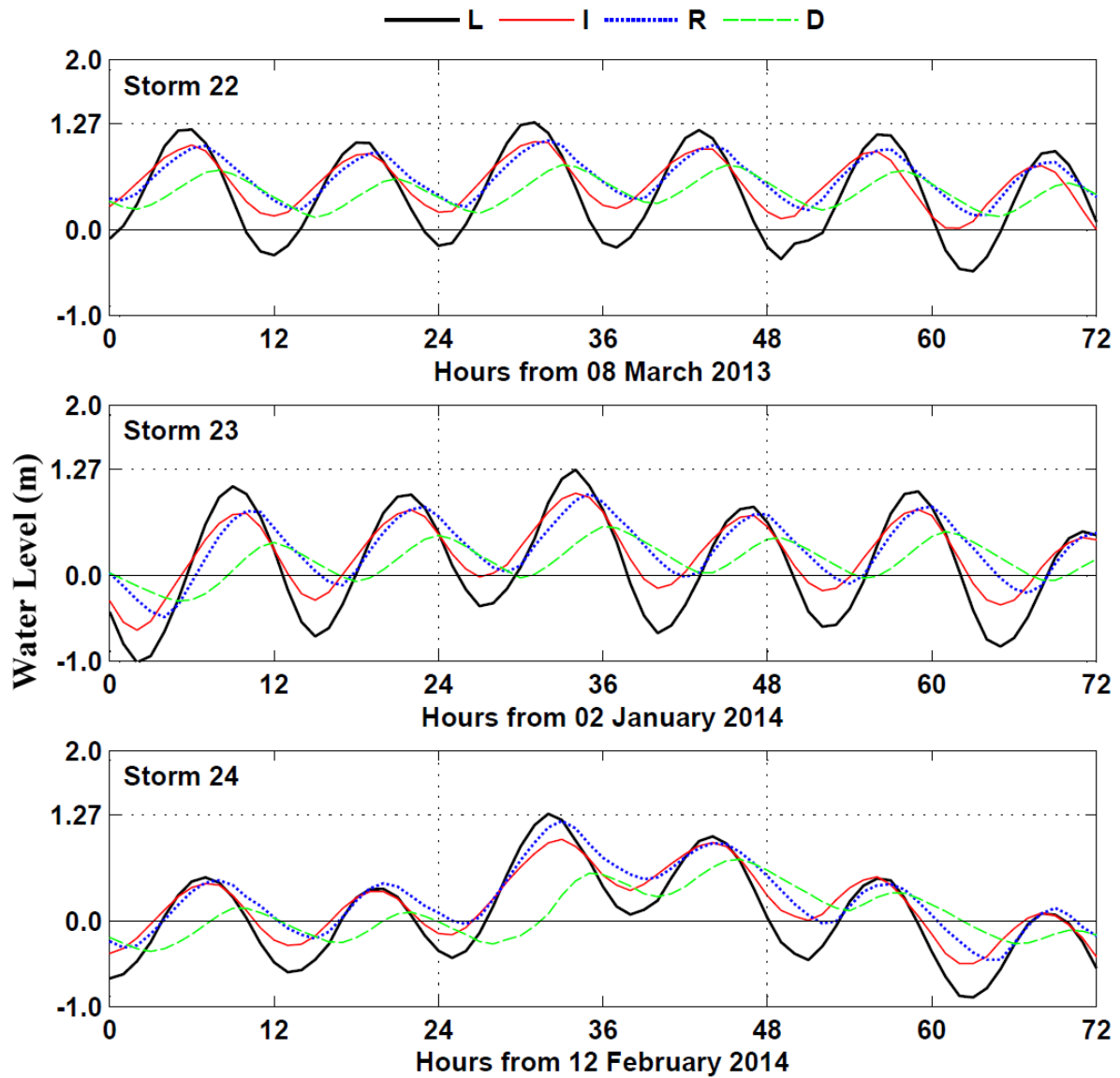


Figure 2.22 3-day time series of water levels at Gauges L, I, R, and D for Storms 22, 23 and 24.

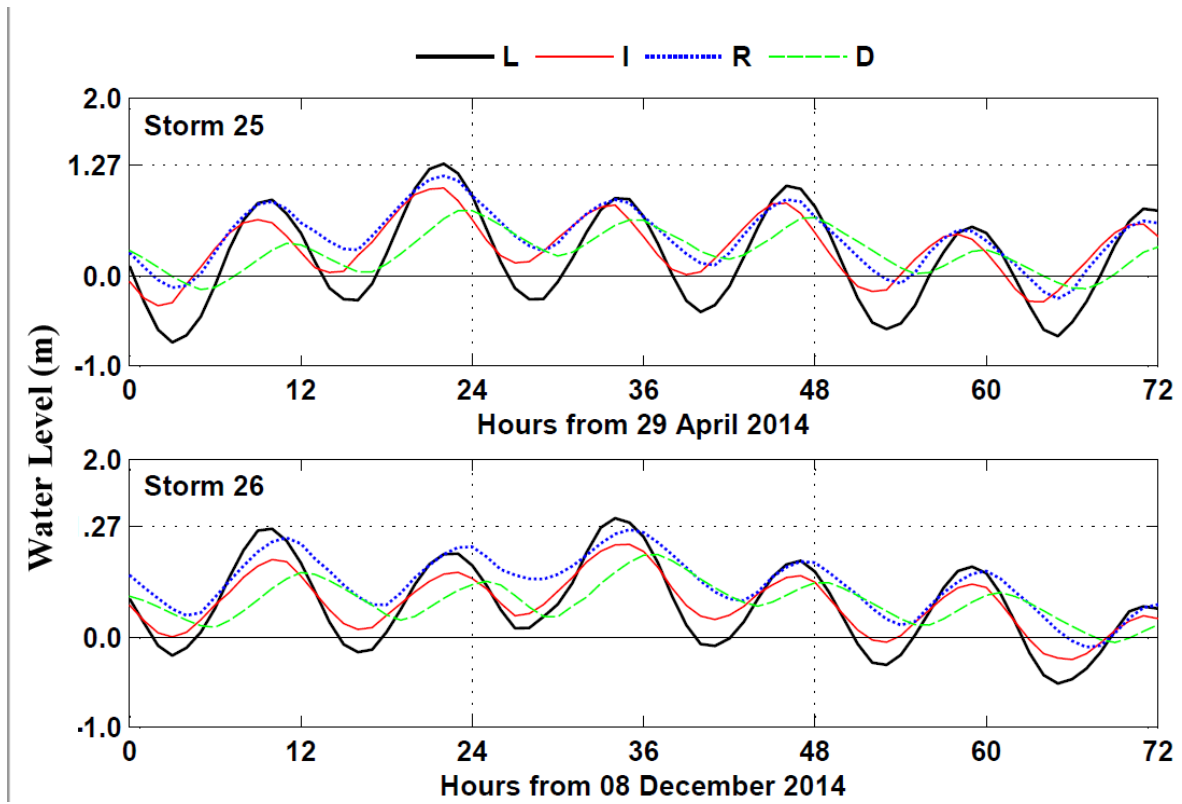


Figure 2.23 3-day time series of water levels at Gauges L, I, R, and D for Storms 25 and 26.

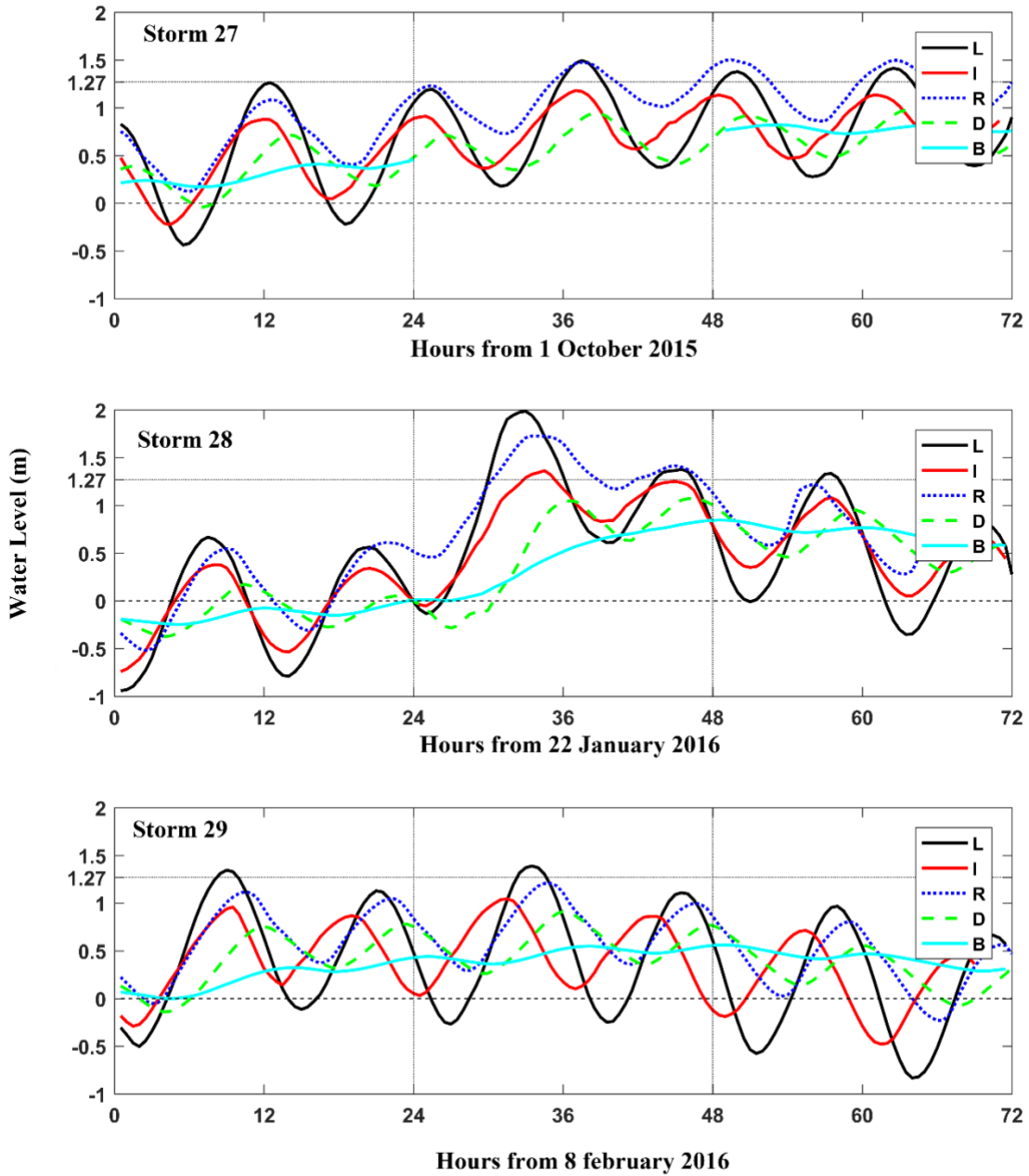


Figure 2.24 3-day time series of water levels at Gauges L, I, R, D and B for Storms 27, 28, and 29.

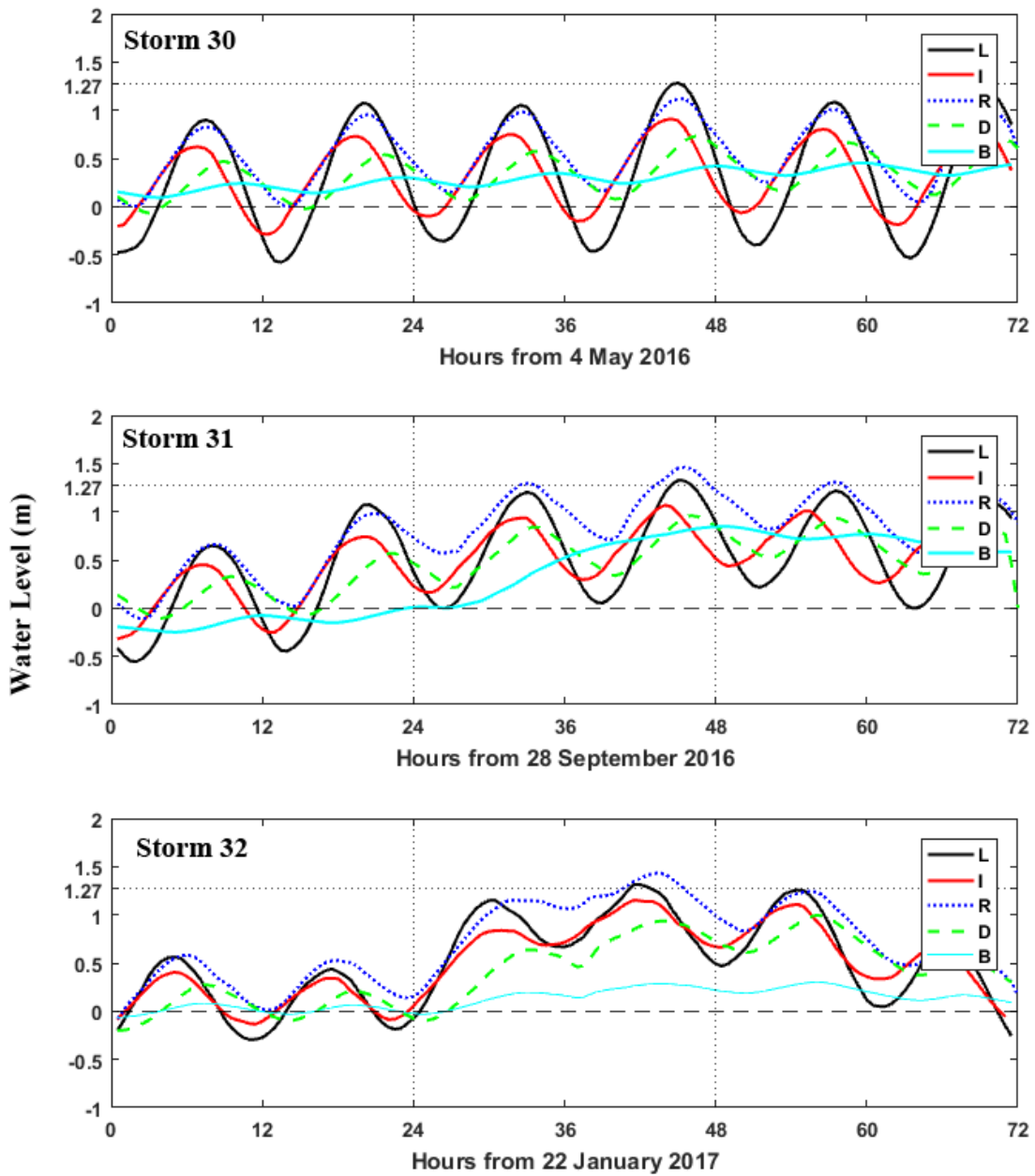


Figure 2.25 3-day time series of water levels at Gauges L, I, R, D and B for Storms 30, 31, and 32.

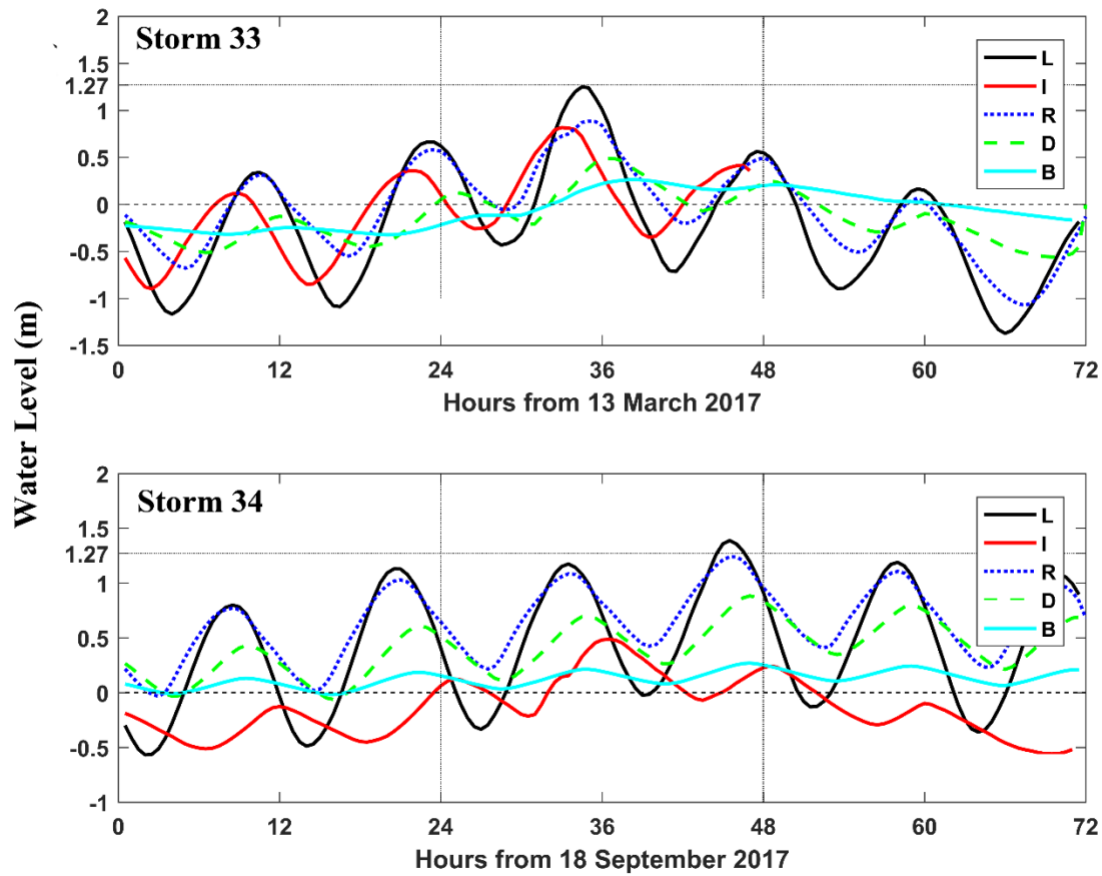


Figure 2.26 3-day time series of water levels at Gauges L, I, R, D and B for Storms 33 and 34.

Gauge I, R, D, and O are exposed to storm tide and the peak water level of the expose gauges occurred within a few hours after the peak water level in the ocean. Gauge B, S, and F are sheltered from storm tide and the peak water levels of the sheltered gauges were delayed noticeably. For some storms, the water level peaks were difficult to pinpoint. As a result, the peak water level η_p for each of the bay gauges was defined as the highest water level during the 3-day duration of each storm.

2.2 River Discharge Data

The daily mean discharge data at Millsboro Pond Outlet (USGS 2016) in Indian River Bay was examined to estimate the effect of river discharge on the bay water level. The daily mean discharge on the day of 34 storms in Table 2.2 was less 22 m³/s except for Storm 13 with its daily mean discharge of 30 m³/s. In following, the river discharge is assumed to be negligible.

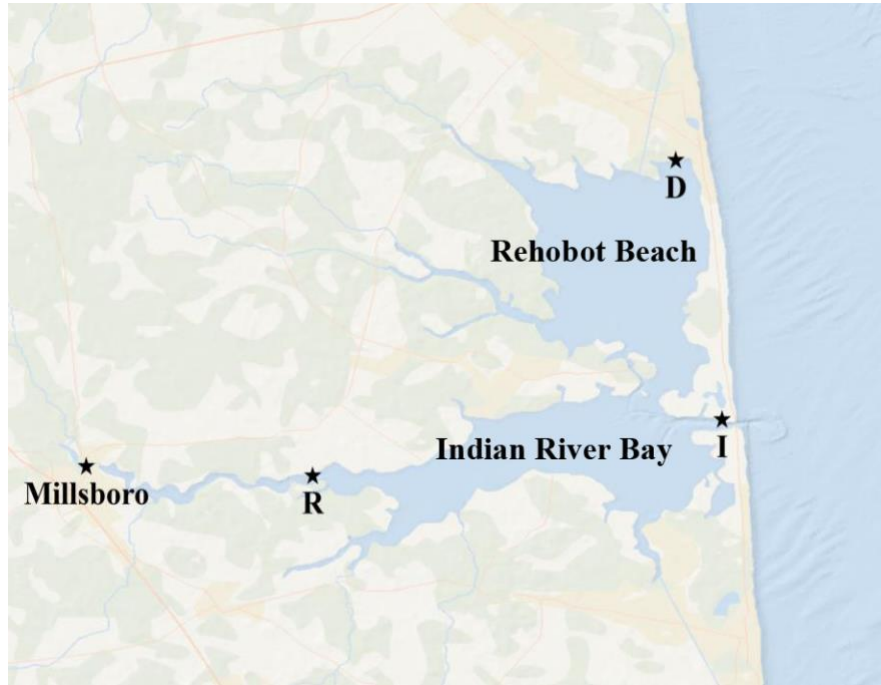


Figure 2.27 Location of Millsboro Pond Outlet.

Table 2.2 Daily mean discharge at Millsboro Pond Outlet

Storm	Daily mean Discharge (m³/s)	Storm	Daily mean Discharge (m³/s)
1	4.36	18	1.73
2	2.43	19	0.91
3	4.61	20	8.77
4	5.69	21	5.58
5	3.54	22	8.09
6	9.00	23	4.27
7	6.59	24	5.63
8	1.36	25	4.30
9	4.30	26	3.00
10	0.88	27	3.45
11	0.48	28	NA
12	2.80	29	4.19
13	30.00	30	3.82
14	7.42	31	21.74
15	11.63	32	3.08
16	1.44	33	6.17
17	1.10	34	2.86

2.3 Offshore Wave Data

Offshore wave data are obtained from the Wave Information Study Stations (WIS) of the U.S. Army Corps of Engineers (USACE 2016). In Figure 2.2 are indicated the WIS locations 63154, 63156, 63158, 63160, 63162, and 63164. Kobayashi and Zhu et al. (2017) analyzed the incident waves for lines L1-L14, in Figure 2.2.

The wave conditions during each storm are represented by the hourly time series of the spectral significant wave height H_{m0} , spectral peak period T_p and vector mean wave angle θ (positive clockwise). The shoreline is inclined at an angle of 6.38° counterclockwise from the north.

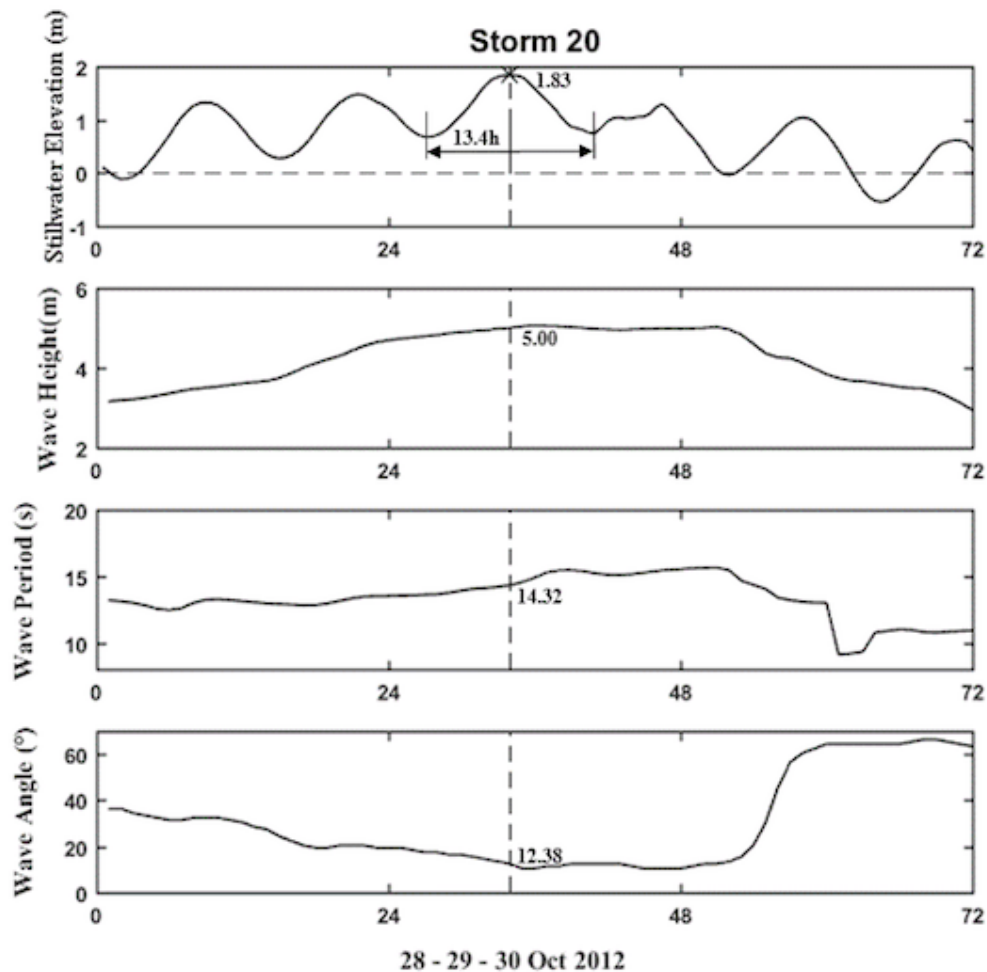


Figure 2.28 3-day time series of water elevation η_0 at tide gauge L, and the wave height H_{m0} , period T_p , and angle θ at WIS 63160 station for storm 20.

Figure 2.28 depicts the 3-day time series of water elevation η_o at the ocean gauge L and wave height H_{mo} , period T_p , and angle θ at WIS 63160 for storm 20, Hurricane Sandy. The maximum η_m of η_o varying with time is 1.85 m and the vertical line indicates the time of $\eta_o = \eta_m$. The wave conditions at the time of peak water elevation η_m at Lewis for storm 20, are given by $H_{mo}=5.00$ m, $T_p= 14,32$ s and $\theta=12.38^\circ$. Hurricane Sandy generated the large storm tide and waves. The surge duration between the two low water levels adjacent to the peak water level at gauge L, present in figure 2.28, is $T_s=13.4$ h. The value of T_s is obtained from the time series of η_o above the datum (NAVD88) in the vicinity of the peak water level.

Table 2.3 shows the values of H_{mo} , T_p and θ at the time of peak water elevation at Lewis, for storms 1 – 26. Wave data for storms 27 – 34 are not available. The ranges were $H_{mo}=0.96 – 5.01$ (m) , $T_p = 4.52 - 14.70$ (s), and $\theta = (-55.62) – 68.38$ ($^\circ$).

Table 2.3 Spectral significant wave height H_{m0} , spectral peak period T_p , and wave angle θ (positive clockwise) from the normal to the straight barrier beach shoreline at the time of the peak water elevation η_m at Lewes.

Storm	Peak Water Level η_m (m)	Wave height H_{m0} (m)	Wave Period T_p (s)	Wave Angle θ(°)
1	1.39	2.06	10.25	-10.62
2	1.32	2.72	10.78	-1.62
3	1.38	0.96	8.11	68.38
4	1.32	1.12	4.52	2.38
5	1.45	4.45	11.61	-1.62
6	1.32	4.61	12.09	3.88
7	1.28	1.85	10.55	-18.62
8	1.27	0.99	8.17	-6.12
9	1.6	1.52	9.81	9.38
10	1.29	3.66	11.30	5.38
11	1.28	3.11	9.60	-13.12
12	1.45	2.83	9.66	-4.62
13	1.6	5.01	13.11	2.88
14	1.38	1.39	4.93	-20.62
15	1.3	2.09	6.27	5.38
16	1.27	1.69	6.93	39.38
17	1.7	3.66	14.35	46.88
18	1.56	1.68	5.72	-14.62
19	1.43	1.52	9.59	-18.62
20	1.85	5.00	14.32	12.38
21	1.45	2.96	7.82	-12.62
22	1.29	2.33	14.70	-23.62
23	1.28	1.79	6.35	-55.62
24	1.3	1.94	6.18	2.38
25	1.3	1.89	6.77	1.38
26	1.36	3.10	13.26	-4.12
Min	1.27	0.96	4.52	-55.62
Max	1.85	5.01	14.70	68.38

Chapter 3

Analytical Model

The analytical model proposed by Kobayashi and Zhu (2017) is used to express the peak water level η_p at each bay gauge location as a function of the corresponding η_m and surge duration T_s at Gauge L for each storm tide. The effects of wind waves and local wind on the water level in Indian River Bay and Rehoboth Bay were examined numerically and found to be small in comparison to storm tide penetrating through the Indian River Inlet (Lu *et al.* 2018). The surface areas of Indian River Bay and Rehoboth Bay are almost equal and the combined surface area, A_B , is approximately 75 km². The surface area of Little Assawoman Bay is about 10 km². The effects of wind waves and local wind on the water level in Little Assawoman Bay are neglected because of its size and enclosure.

3.1 Governing Equation

The analytical model was based on the conservation equation of water volume in a bay and a hydraulic energy equation for flow in a tidal inlet. The temporal variation of the water level in the ocean was simplified and expressed using the peak water level η_m and surge duration T_s . The effect of wave overtopping over a barrier beach between the ocean and bay was included and represented by the peak wave overtopping rate Q_m . The peak water level η_p in the bay with its surface area A_B was expressed as:

$$\eta_p = \frac{\eta_m}{\sqrt{1 + \beta^2}} \left(1 + \frac{\beta Q_m^*}{\pi} \right) \quad ; \quad Q_m^* = \frac{T_s Q_m}{\eta_m A_B}$$

EQUATION (1)

where the dimensionless wave overtopping rate Q_m^* compares the contributions of wave overtopping and storm tide through the inlet. The dimensionless parameter β was expressed as

$$(2\beta^2 + 1)^2 = (K^* \eta_m^*)^2 + 1 \quad ; \quad \eta_m^* = \frac{\eta_m}{g T_s^2} \times 10^{10}$$

EQUATION (2)

where g is the gravitational acceleration and the surge steepness parameter η_m^* was of the order of unity for the 34 storms during 2005-2017. The dimensionless parameter K^* is related to the characteristics of the inlet and bay.

Kobayashi and Zhu (2017) calibrated K^* for Gauge I, R, and D in Indian River Bay and Rehoboth Bay for 27 storms during 2005-2015. For each of the three bay gauges, the value of β in Equation 1 with $Q_m^*=0$ and K^* in Equation 2 were calculated using the measured values of η_p for each of the 27 storms with the known values η_m and T_s . The average value of K^* for the 27 storms was used to represent the degree of damping and time lag for storm tide propagating from Gauge L to Gauge I, R, and D. The calibration of K^* using the data of each bay gauge compensated the shortcoming of the analytical model.

Wave overtopping of the barrier beach between the ocean and bay occurred during Storm 20 (S20) which was Hurricane Sandy in 2012. Kobayashi and Zhu (2017) used a numerical model to estimate $Q_m=1,380$ m³/s for the barrier beach of 7.2 km alongshore length for the combined area $A_B=75$ km² of the two bays. Equation 1 with the average K^* was used to predict η_p for $Q_m=0$ (no wave overtopping) and $Q_m=1,380$ m³/s. The analytical model including wave overtopping improved the agreement between the measured and predicted η_p for Gauge D and I situated close to the barrier beach and worsened the agreement for Gauge R situated away from the barrier beach. Lu *et al.* (2018) computed the horizontal spreading of overtopping water inside Rehoboth Bay and Indian River Bay. Their computed spreading indicated little wave overtopping effect in the vicinity of Gauge R. In this study, Equation 1 with the measured η_p is used later to estimate the corresponding Q_m for each of the bay gauges.

Chapter 4

Model Calibration

The parameter K^* at each bay gauge was calibrated using the 34 storms during 2005-2017 on the basis of the calibration procedure of Kobayashi and Zhu (2017). The calibrated results for Gauge I, R, D, and B are shown in Figure 4.1. The measured ratios between the peak water level η_p and η_m are plotted as a function of the surge steepness parameter η_m^* . The analytical ratio based on Equation 1 and 2, with $Q_m=0$, is plotted for the minimum, average, and maximum values of the calibrated K^* . Data points above the minimum K^* and below the maximum K^* were excluded from averaging the calibrated values of K^* . Gauge I has one outlier point and Gauge R has three outlier points. The causes of these outlier points are uncertain but are not related to Hurricane Sandy (S20) denoted by a solid circle. Gauge B installed in 2015 has only eight data points. For Gauge I, R, and D, the range and average value of the calibrated K^* are practically the same for the 34 storms during 2005-2017 and 27 storms during 2005-2015. The average value of K^* is 1.6, 1.3, 5.3, and 11.2 for Gauge I, R, D, and B, respectively.

Damping of the peak water level increases with increase of K^* . Storm tide in the ocean propagates through the Indian River Inlet and reaches Gauge I, R, D, and B. The average K^* at Gauge D is increased by a factor of about 4 because of additional damping through the ditches between Indian River Bay and Rehoboth Bay. The average K^* at Gauge B is increased by a factor of about 8 because of strong damping in the canal and ditch between Indian River Bay and Gauge B.

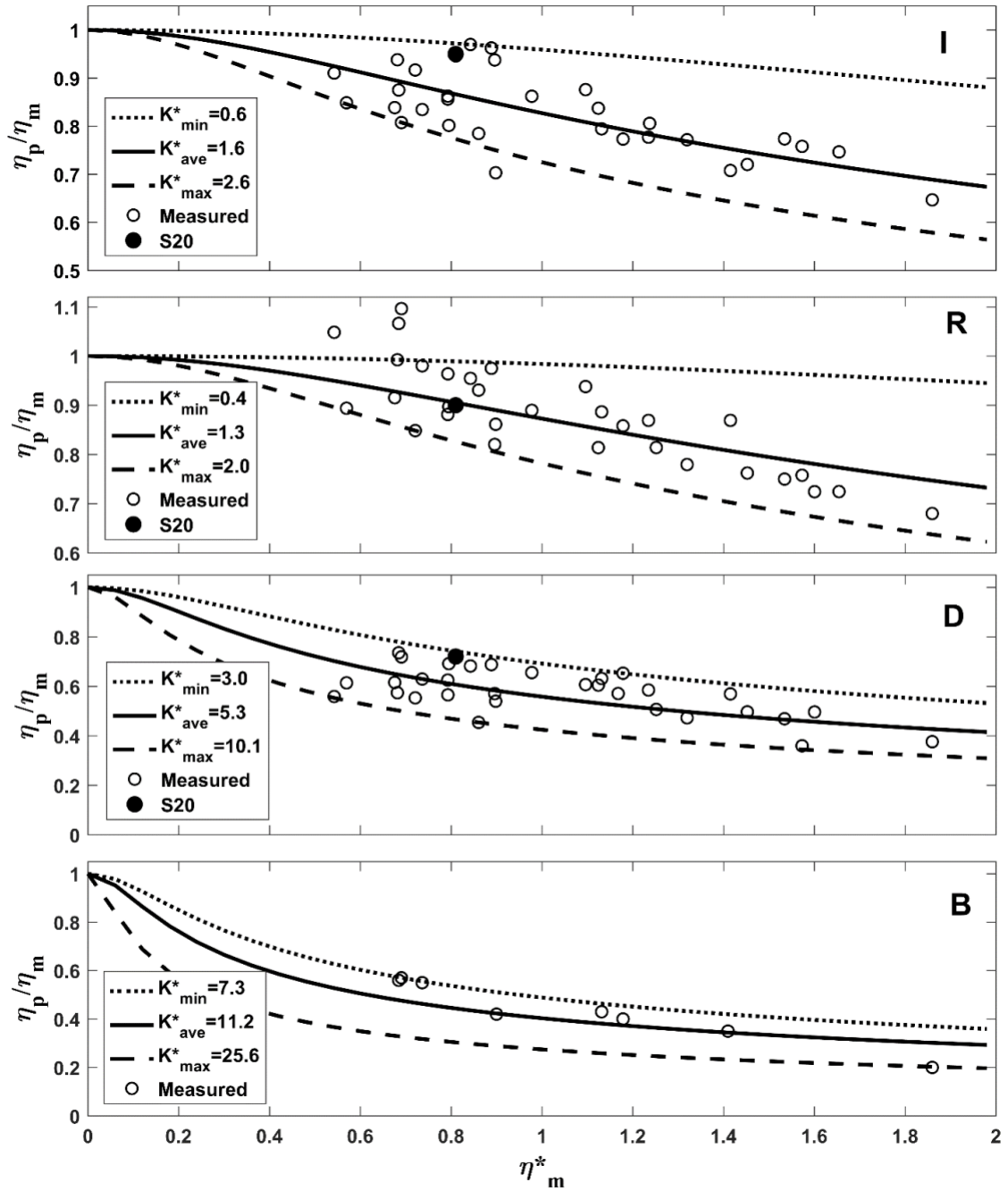


Figure 4.1 Measured and analytical peak water level ratio (η_p/η_m) as a function of surge steepness parameter η_m^* for range of inlet and bay parameter K^* at Gauge I, R, D, and B.

Figure 4.2 shows the calibrated results for Gauge O, F and S. One outlier point above the minimum K^* for Gauge O is not related to Hurricane Sandy (S20). One outlier point for Gauge F and S in Little Assawoman Bay is associated with Hurricane Sandy. The town of South Bethany west of Delaware Route 1 on the barrier beach between the Atlantic Ocean and Little Assawoman Bay was flooded during Hurricane Sandy (USACE 2015). Delaware Route 1 was closed for many hours. The average value of K^* is 5.1, 15.4, and 14.4 for Gauge O, F, and S, respectively. Larger damping from Gauge L to Gauge O ($K^*=5.1$) than to Gauge I ($K^*=1.6$) suggests that the water level of Gauge L may not represent the ocean water level for Gauge O adequately. The average values of K^* for Gauge F and S are very similar, indicating little damping within Little Assawoman Bay. Strong damping through the ditch between Assawoman Bay and Little Assawoman Bay increases the average K^* from 5.1 to about 15. The average $K^*=11.2$ for Gauge B is smaller than the average K^* for Gauge F and S. This suggests that the water level at Gauge B is affected mostly by the water level in Indian River Bay.

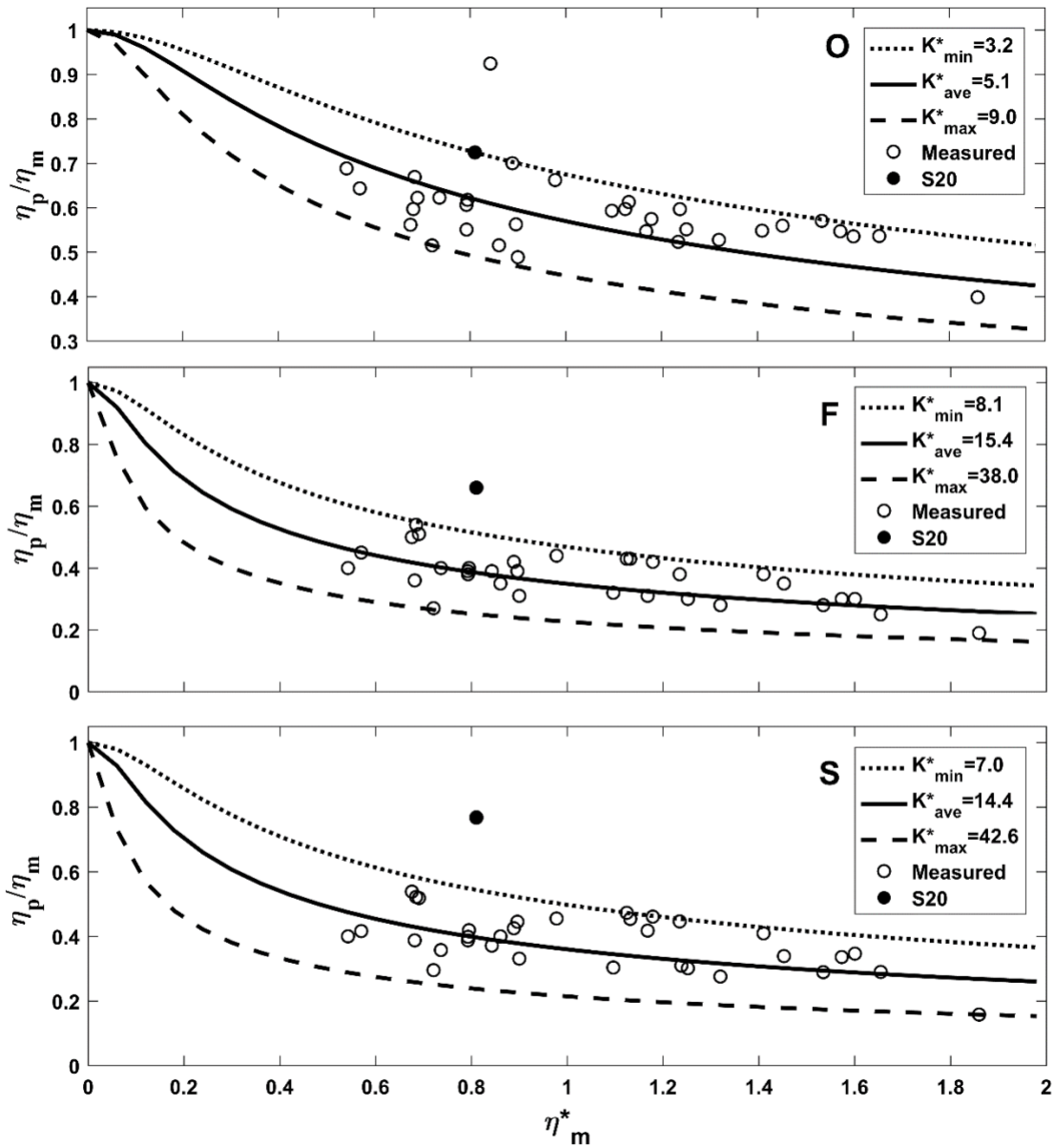


Figure 4.2 Measured and analytical peak water level ratio (η_p/η_m) as a function of surge steepness parameter η_m^* for range of inlet and bay parameter K^* at Gauge O, F, and S.

Chapter 5

MODEL ACCURACY

The analytical model with $Q_m=0$ and the average K^* is used to predict the peak water level η_p at each bay gauge for the 34 storms. Figure 5.1 shows the measured and predicted peak water level η_p at Gauge I, R, D, and B. The deviation of data points from the solid line of perfect agreement is indicated by two dashed lines above and below the solid line. The deviation is 18, 14, 23, and 14 cm for Gauge I, R, D, and B, respectively. The RMS relative error E is the standard deviation of the relative error between the measured and predicted values. The value of E increases with the increase of the average K^* because the small measured values are difficult to predict accurately. For the data point of Hurricane Sandy (S20), the analytical model with $Q_m=0$ predicts the measured η_p of Gauge R but underpredicts the measured η_p of Gauge I and D by about 0.2 m.

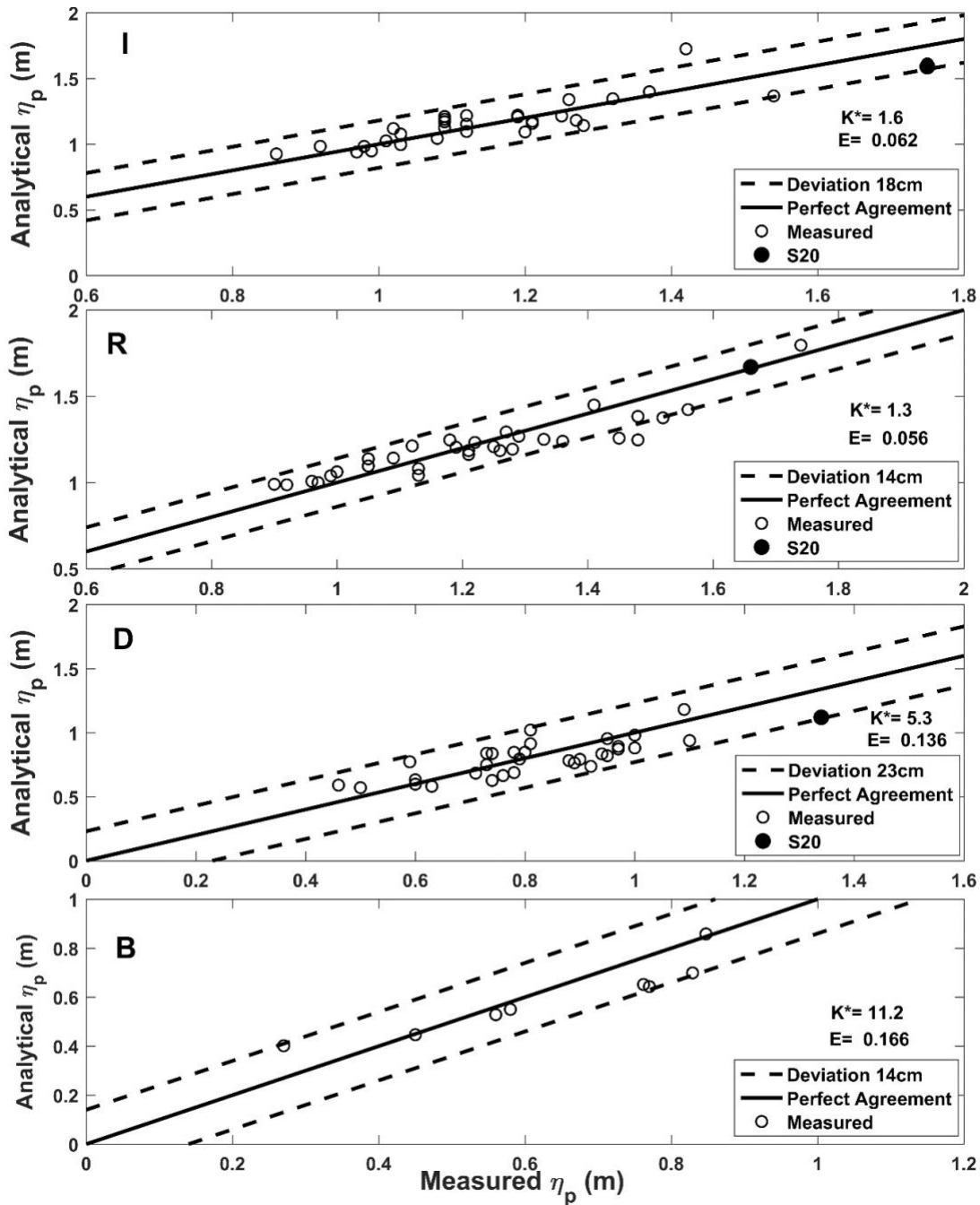


Figure 5.1 Measured and analytical peak water level η_p at Gauge I, R, D, and B and RMS relative error E .

Figure 5.2 shows the comparison for Gauge O, F, and S. The scatter of data points about the solid line of the perfect agreement appears to be large for Gauge F and S because of the relatively small measured values. The degree of agreement in terms of the deviation and RMS relative error is similar in Figures 5.1 and 5.2. The analytical model with $Q_m=0$ underpredicts the

measured η_p during Hurricane Sandy. The data point of S20 for Gauge F and S is well beyond the deviation of about 0.2 m. Little Assawoman is almost enclosed and wave overtopping of the barrier beach can lead to accumulation of overtopped water in the bay with limited water outflux through the ditch.

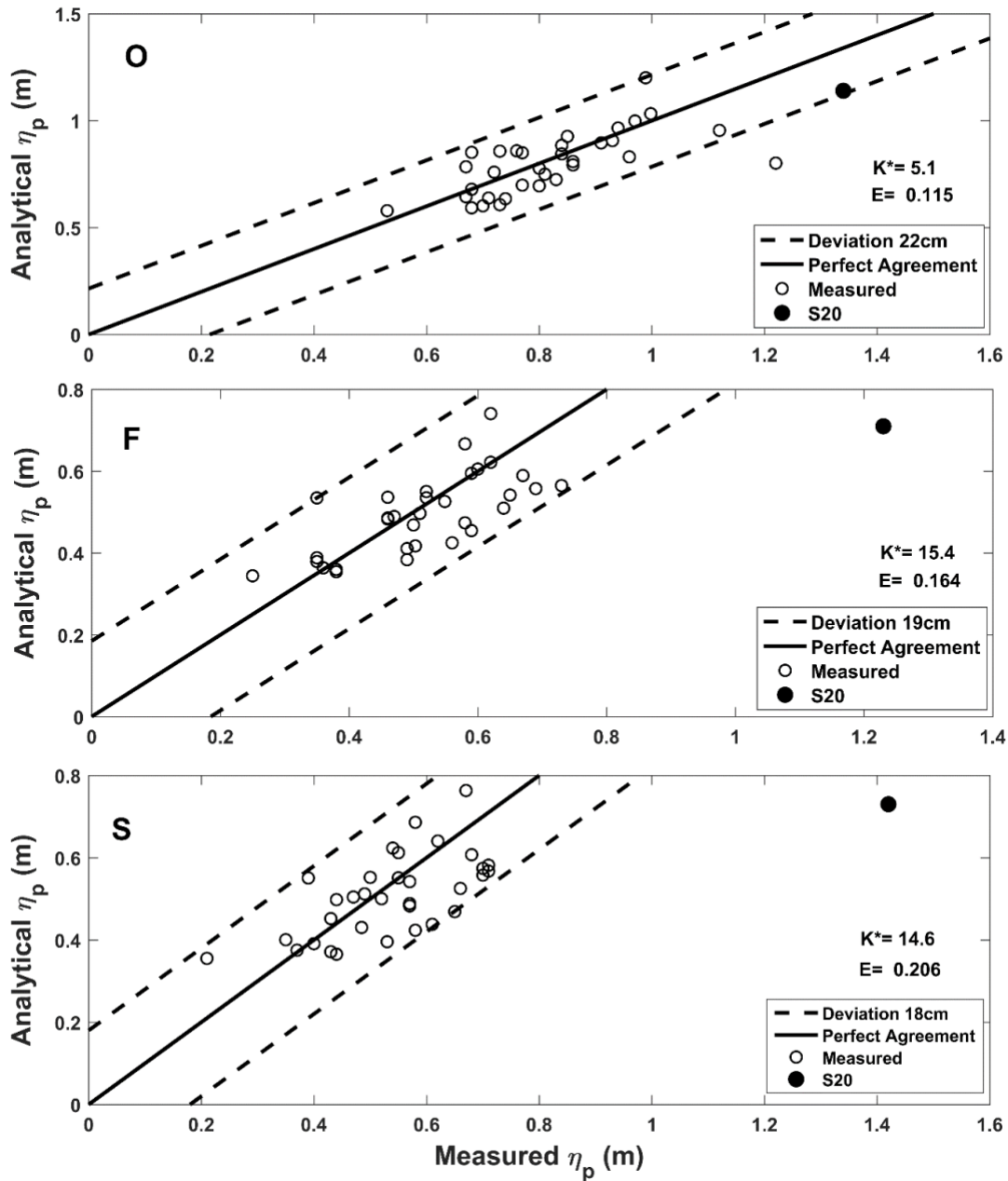


Figure 5.2 Measured and analytical peak water level η_p at Gauge O, F, and S and RMS relative error E .

Chapter 6

WAVE OVERTOPPING

The peak wave overtopping rate Q_m is estimated using Equations 1 and 2 with the average K^* and measured η_p at each bay gauge. For Hurricane Sandy, $\eta_m=1.85$ m, $T_s=13.4$ h, and $\eta_m^*=0.81$ at Gauge L. Table 1 lists the measured η_p at Gauge I, R, D, O, F, and S. The average K^* for each of these gauges is indicated in Figures 5.1 and 5.2. The surface area A_B is 75 km² for Gauge I, R, and D and 10 km² for Gauge O, F, and S. Gauge O is not in Little Assawoman Bay but might have been affected by the outflux of overtopped water through the ditch. The dimensionless rate Q_m^* indicates the degree of importance of wave overtopping in comparison with storm tide through the inlet or ditch. The contribution of wave overtopping to the peak water level η_p is important for Gauge F and S in Little Assawoman Bay and noticeable for Gauge I and D close to the barrier beach in Indian River Bay and Rehoboth Bay, respectively. The computed value of Q_m^* is slightly negative for Gauge R located on the western end of Indian River Bay. The computed Q_m^* for Gauge O is larger than expected and discussed below.

Table 6.1 lists the estimated values Q_m for Gauge I, R, D, O, F, and S. For Gauge R, $Q_m=0$ because Q_m must be positive or zero. The estimated values need to be interpreted physically. For Indian River Bay and Rehoboth Bay, the estimated peak overtopping rate is approximately $1,350$ m³/s and almost the same as the computed value of $1,380$ m³/s by Kobayashi and Zhu (2017) using their numerical model for wave overtopping of the barrier beach. However, overtopping water may not have reached the vicinity of Gauge R as computed by Lu *et al.* (2018) using their numerical model for storm tide including wave overtopping. For Little Assawoman Bay, the estimated peak overtopping rate is about 430 m³/s for the smaller surface area of this bay. This estimated rate will need to be verified using a numerical wave overtopping model. For Gauge O, the estimated rate of 164 m³/s is relatively small but may not be real in light of the accuracy of the analytical model. The measured η_p for S20 at Gauge O in Figure 5.2 is within the deviation of 22 cm from the analytical η_p with $Q_m=0$. Equation 1 cannot predict whether wave overtopping occurs or not. The occurrence of wave overtopping needs to be confirmed for the use of Equation 1 to estimate Q_m .

Table 6. Estimated Peak Wave Overtopping Rate Q_m at Gauge I, R, D, O, F, and S during Strom 20.

Gauge	I	R	D	O	F	S
$\eta_p(\text{m})$	1.75	1.66	1.34	1.34	1.23	1.42
Q_m^*	0.48	-0.04	0.46	0.43	0.95	1.28
$Q_m(\text{m}^3/\text{s})$	1379	0	1322	164	365	489

Chapter 7

Conclusions

Storm tide in inland bays with complex bathymetry is difficult to predict accurately partly because of the difficulty in resolving detailed bathymetry including ditches and canals. A simple approach based on the analytical model for peak water levels was proposed by Kobayashi and Zhu (2017) for inland bays with several tide gauges in operation for a decade or longer. Tide gauge data at the mouth of a large bay with a wide mouth was used to identify 34 storms in the ocean during 2005-2017. The peak water level and surge duration were used to characterize each storm. The peak water levels at seven tide gauges inside the inland bays were used to examine storm tide propagation and damping. The dimensionless parameter at each gauge location was calibrated for the 34 storms. This parameter determines the degree of the peak water level damping at each gauge location. The analytical model with the calibrated parameter was shown to predict the peak water levels at the seven gauge locations within errors of about 0.2 m except for Hurricane Sandy in 2012. The analytical model including wave overtopping was used to estimate the peak wave overtopping rate corresponding to the measured peak water level inside each bay next to the barrier beach. The estimated rate for one bay was consistent with the rate computed using a numerical wave overtopping model. The proposed approach is useful in analyzing tide gauge data and predicting peak water levels during storms.

REFERENCE

- Cialone M. A., A. S. Grzegorzewski, D.J. Mark, M.A. Bryant, and T. C. Massey, 2017. "Coastal-storm model development and water-level validation for the North Atlantic Coast Comprehensive Study". *J. Waterway, Port, Coastal, and Ocean Engineering*, 143(5), 04017031, 1-16.
- Johnson B. D., N. Kobayashi, and K.D. Watson, 1994. "Flooding of Delaware Route 54 between Little Assowoman and Assowoman Bays due to storm surge and tides". *Research Report No. CACAR-94-16, Center for Applied Coastal Research, University of Delaware, Newark, Delaware.*
- Kobayashi N., and T. Zhu, 2017. " Bay flooding through tidal inlet and by wave overtopping of barrier beach". *J. Waterway, Port, Coastal and Ocean Engineering*, 143(5), 04017024, 1–14.
- Lu Y., F. Shi, N. Kobayashi, M. Malej, T. Zhu, and W. Feng, 2018. "Numerical investigation of excessive surge induced by wave overtopping in an inlet-bay system". *Coastal Engineering*, 140, 383–394.
- Nadal-Caraballo, N. C., J.A. Melby, and V.M. Gonzalez, 2016. "Statistical analysis of historical extreme water levels for the U.S. North Atlantic coast using Monte Carlo life-cycle simulation". *J. Coastal Research*, 32(1), 35–45.
- U.S. Army Corps of Engineers (USACE), 2015. "North Atlantic Coast Comprehensive Study: Resilient adaptation to increasing risk."
<https://www.nad.usace.army.mil/CompStudy/>

U.S. Department of Commerce, National Oceanic and Atmospheric Administration (NOAA),
2018. "Center for Operational Oceanographic Products and Service."

<https://tidesandcurrents.noaa.gov>

U. S. Geological Survey (USGS), 2018. "National waters Information System: Mapper."
<https://maps.waterdata.usgs.gov/mapper/index.html>